Pontifícia Universidade Católica
do Rio de Janeiro

Ingrid Pires Macedo Oliveira dos Santos

Analysis and Modeling of Torsional Vibrations and Stick-Slip Phenomenon in Slender Structure Systems: Experimental Investigations and Nonlinear Identification

Tese de Doutorado

Thesis presented to the Programa de Pós–graduação em Engenharia Mecânica, do Departamento de Engenharia Mecânica da PUC-Rio in partial fulfillment of the requirements for the degree of Doutor em Engenharia Mecânica.

Advisor : Prof. Helon Vicente Hultmann Ayala
Co-advisor: Prof. Hans Ingo Weber

Rio de Janeiro
August 2023

Pontifícia Universidade Católica
do Rio de Janeiro

Ingrid Pires Macedo Oliveira dos Santos

Analysis and Modeling of Torsional Vibrations and Stick-Slip Phenomenon in Slender Structure Systems: Experimental Investigations and Nonlinear Identification

Thesis presented to the Programa de Pós–graduação em Engenharia Mecânica da PUC-Rio in partial fulfillment of the requirements for the degree of Doutor em Engenharia Mecânica. Approved by the Examination Committee:

Prof. Helon Vicente Hultmann Ayala
Advisor
Departamento de Engenharia Mecânica – PUC-Rio

Prof. Hans Ingo Weber
Co-advisor
Departamento de Engenharia Mecânica – PUC-Rio

Dr. Fredy Jonel Coral Alamo
Kongsberg Maritime

Prof. Igor Braga de Paula
Departamento de Engenharia Mecânica – PUC-Rio

Prof. Marco Antonio Meggiolaro
Departamento de Engenharia Mecânica – PUC-Rio

Dr. Romulo Reis Aguiar
Schlumberger Serviços de Petróleo-BRGC

Rio de Janeiro, August the 23rd, 2023

Ingrid Pires Macedo Oliveira dos Santos

Ingrid Pires graduated in mechanical engineering in 2017 from UFRJ and got her master's degree in 2019 from PUC-Rio. This DSc. thesis was done at PUC-Rio and at the University of Aberdeen (Scotland).

Bibliographic data

Santos, Ingrid Pires Macedo Oliveira dos

Analysis and Modeling of Torsional Vibrations and Stick-Slip Phenomenon in Slender Structure Systems: Experimental Investigations and Nonlinear Identification / Ingrid Pires Macedo Oliveira dos Santos; advisor: Helon Vicente Hultmann Ayala; co-advisor: Hans Ingo Weber. – 2023.

82 f: il. color. ; 30 cm

Tese (doutorado) - Pontifícia Universidade Católica do Rio de Janeiro, Departamento de Engenharia Mecânica, 2023.

Inclui bibliografia

1. Engenharia Mecânica – Teses. 2. Sistemas Dinâmicos e Controle – Teses. 3. Vibrações torsionais. 4. Fenômeno stick-slip. 5. Testes experimentais. 6. Dinâmica não linear. 7. Bit bouncing. I. Hultmann Ayala, Helon Vicente. II. Weber, Hans Ingo. III. Pontifícia Universidade Católica do Rio de Janeiro. Departamento de Engenharia Mecânica. IV. Título.

CDD: 621

Acknowledgments

I am thankful to my family, and friends for their unwavering support.

Special thanks to Professor Hans Weber for six years of dedicated guidance and friendship.

Thanks to Professor Helon Ayala for his valuable input and guidance.

I appreciate the valuable contributions and teamwork from LabVib colleagues, especially Dr. Mariana Gomes and Dr. Eduardo Goecoechea.

Thanks to Professor Marian Wiercigroch for his supervision during my time in Aberdeen and to CADR colleagues for their teamwork and support.

Finally, I acknowledge the examiners of this thesis for their time, expertise, and critical evaluation of this work.

This study was made possible through the funding provided by CNPQ, CAPES, and PUC-Rio.

This study was financed in part by the Coordenação de Aperfeiçoamento de Pessoal de Nível Superior – Brasil (CAPES) – Finance Code 001.

Abstract

Santos, Ingrid Pires Macedo Oliveira dos; Hultmann Ayala, Helon Vicente (Advisor); Weber, Hans Ingo (Co-Advisor). **Analysis and Modeling of Torsional Vibrations and Stick-Slip Phenomenon in Slender Structure Systems: Experimental Investigations and Nonlinear Identification**. Rio de Janeiro, 2023. 82p. Tese de Doutorado – Departamento de Engenharia Mecânica, Pontifícia Universidade Católica do Rio de Janeiro.

During drilling for oil extraction purposes, the drill string experiences complex dynamic behavior, and this work delves into the experimental study and the mathematical modeling of such behavior. Self-excited vibrations, such as axial, lateral, and torsional vibrations, which can lead to detrimental effects such as bit bouncing, whirling, and torsional stick-slip are highlighted in this thesis.

Distinct aspects of drilling dynamics are considered in this investigation to enhance the understanding of various phenomena. Initially, an experimental analysis of a lab-scale rig is conducted, providing valuable insights into the dynamics of such systems. And the influence of control parameters on the system's response is examined, particularly in identifying the conditions under which the stick-slip phenomenon is likely to occur.

Secondly, the thesis proposes system identification strategies for nonlinear systems, specifically focusing on the same laboratory test rig. An innovative ensemble approach is proposed, which combines gray and black-box modeling techniques to effectively calibrate the parameters of a dynamical system, particularly those associated with friction. This approach improves prediction accuracy compared to traditional gray-box methods while maintaining interpretability in the dynamic responses. Furthermore, the research employs physics-informed deep learning to estimate the low-dimensional model mechanical and friction parameters. Calibration using experimental data obtained from a specialized setup provides insights into the drill-string system's behavior.

Finally, the thesis involves experimental investigations on the coupling between torsional and axial oscillations using a modified and adapted lab-scale drilling rig equipped with real drill bits and rock samples.

In summary, this thesis advances our understanding of drill-string dynamics and presents helpful applications for system identification techniques.

Keywords

Torsional vibrations; Stick-slip phenomenon; Experimental tests; Nonlinear dynamics; Bit bouncing.

Resumo

Santos, Ingrid Pires Macedo Oliveira dos; Hultmann Ayala, Helon Vicente; Weber, Hans Ingo. **Análise e Modelagem de Vibração Torcional e Stick-Slip em Sistemas de Estruturas Esbeltas: Investigações Experimentais e Identificação Não Linear**. Rio de Janeiro, 2023. 82p. Tese de Doutorado – Departamento de Engenharia Mecânica, Pontifícia Universidade Católica do Rio de Janeiro.

Durante a perfuração de poços de petróleo, a coluna de perfuração apresenta um comportamento dinâmico complexo, esta tese foca no estudo experimental e na modelagem matemática deste comportamento. Neste trabalho, destaca-se as vibrações autoexcitadas axiais, laterais e torcionais, que podem levar a efeitos como o bit bouncing, o whirling e stick-slip torcional.

A primeira contribuição desta tese é a análise experimental de um bancada de testes, que fornece informações sobre a dinâmica de sistemas torcionais. A influência dos parâmetros de controle não lineares na resposta do sistema é investigada, identificando as condições sob as quais o fenômeno stick-slip ocorre.

Em segundo lugar, a tese propõe estratégias de identificação de sistemas para sistemas não lineares, utilizando a mesma bancada de testes supracitada. Uma abordagem híbrida para a identificação é proposta, onde técnicas de modelagem de caixa cinza e caixa preta são combinadas para calibrar os parâmetros do sistema, particularmente aqueles associados ao atrito. Essa abordagem aumenta a precisão das estimativas em comparação com os métodos tradicionais de caixa cinza, mantendo a interpretabilidade. Além disso, a pesquisa emprega physics-informed deep learning para estimar os parâmetros mecânicos e de atrito do modelo de dois graus de liberdade. A calibração usando dados experimentais obtidos de uma bancada de testes fornece informações sobre o comportamento de sistemas de perfuração.

Finalmente, a tese apresenta investigações experimentais sobre o acoplamento entre oscilações torcionais e axiais utilizando uma bancada experimental de perfuração em escala de laboratório modificada e adaptada equipada com brocas e amostras de rocha reais.

Em resumo, esta tese aumenta a compreensão da dinâmica de colunas de perfuração e apresenta aplicações úteis para técnicas de identificação de sistemas na análise de oscilações torcionais e axiais.

Palavras-chave

Vibrações torsionais; Fenômeno stick-slip; Testes experimentais; Dinâmica não linear; Bit bouncing.

Table of contents

List of figures

List of tables

in your light do we see light.

Psalm 36:9

1 Introduction

The global demand for oil and gas has been on the rise in recent years [1]. After experiencing a historic decline due to the Covid-19 pandemic, as evidenced by the negative growth depicted in the 2020 data on the graph shown in Fig. 1.1, the industry has rebounded, and forecasts indicate further growth in the coming years. It is projected that global liquid fuel consumption will increase by 1.6 million barrels per day (b/d) in 2023, following an average of 99.4 million b/d in the previous year. Additionally, consumption is expected to rise by another 1.7 million b/d in 2024, with much of this growth driven by non-OECD countries [2].

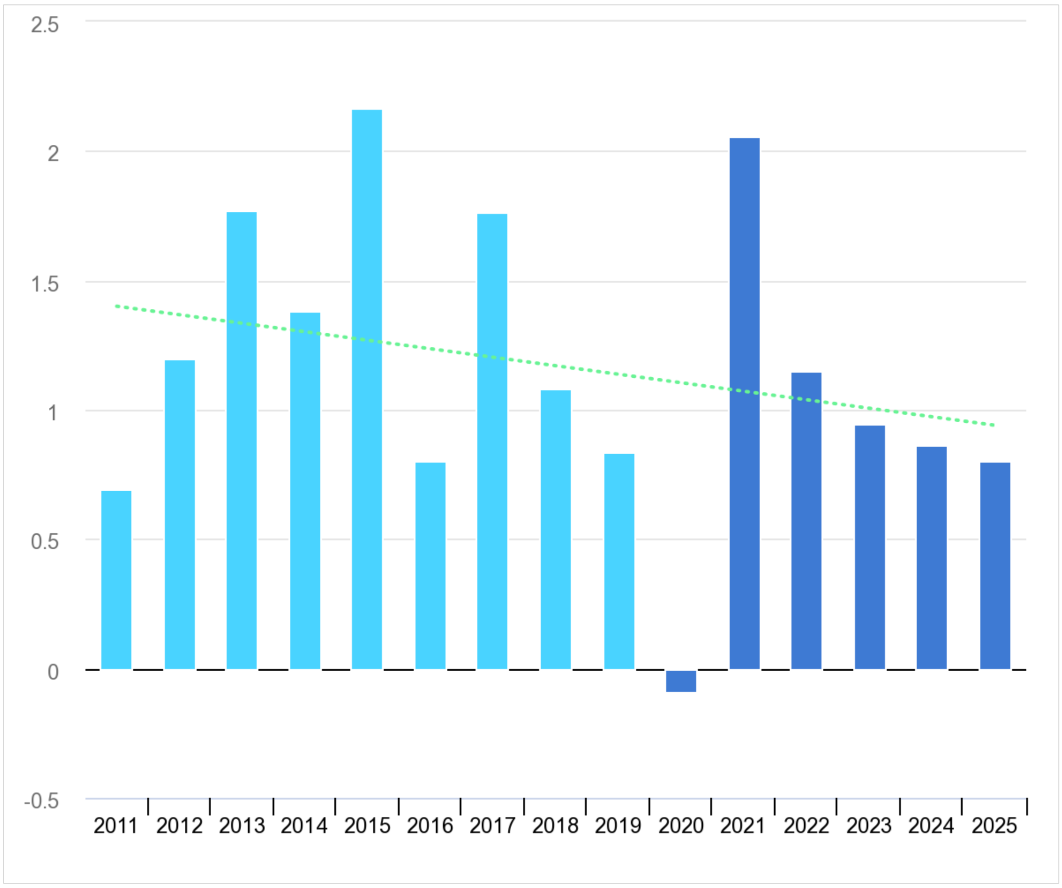

Figure 1.1: Global oil demand growth, 2011-2025 (light blue: historical, dark blue: forecast, and green: trend)[1].

While immediate demand continues to rise, the long-term outlook is uncertain due to factors such as the emergence of alternative fuels and changes in driver and commuter behavior. In this context, the cost of production plays a crucial role. Drilling, in particular, poses significant challenges and expenses in the oil and gas exploration industry. It accounts for approximately 40% of all production costs [3]. As a result, optimizing drilling operations and reducing costs remain key priorities for the industry.

Drilling systems play a crucial role in extracting various resources from the Earth's surface, including water, oil, natural gas, mineral resources, and geothermal energy. This thesis specifically focuses on drilling systems used in oil-field operations. In the past, the drilling process involved raising and dropping a cable tool to percussively drill wells. However, in the 20th century, rotary drilling systems emerged as the predominant method. These systems enabled drilling boreholes to greater depths and with increased efficiency compared to cable tools. While oil also holds significance in the petrochemical industry, its primary role lies as a vital energy source [4].

Drilling wells for oil and gas exploration involves the use of a drill string, which is a set of equipment that undergoes complex dynamic behavior during operation. This thesis delves into the analysis of vibrations in drilling systems, specifically focusing on the experimental exploration of nonlinear dynamics within the drilling process and the development of mathematical models to understand these vibrations. The experimental arrangements employed in this research effectively replicate certain nonlinear dynamics observed in actual drilling rigs, motivating their usage. While this chapter provides an overview of the entire thesis, the subsequent chapters offer more comprehensive literature surveys relevant to each specific topic.

1.1
Drilling dynamics

Drilling systems are essential for extracting oil and natural gas from the ground. Figure 1.2 provides a schematic representation of a drilling system, which can be divided into two main sections: the top drive and the drill string. The focus of this thesis is on the drill string, which connects the motor to the drill bit and is responsible for transmitting rotation and the necessary Weight On Bit (WOB) during drilling operations [5].

During the drilling process, self-excited vibrations can occur, including axial, lateral, and torsional vibrations. These vibrations can lead to detrimental effects such as bit bouncing, whirling, and torsional stick-slip, which can cause premature failures of drilling components. This work specifically focuses on

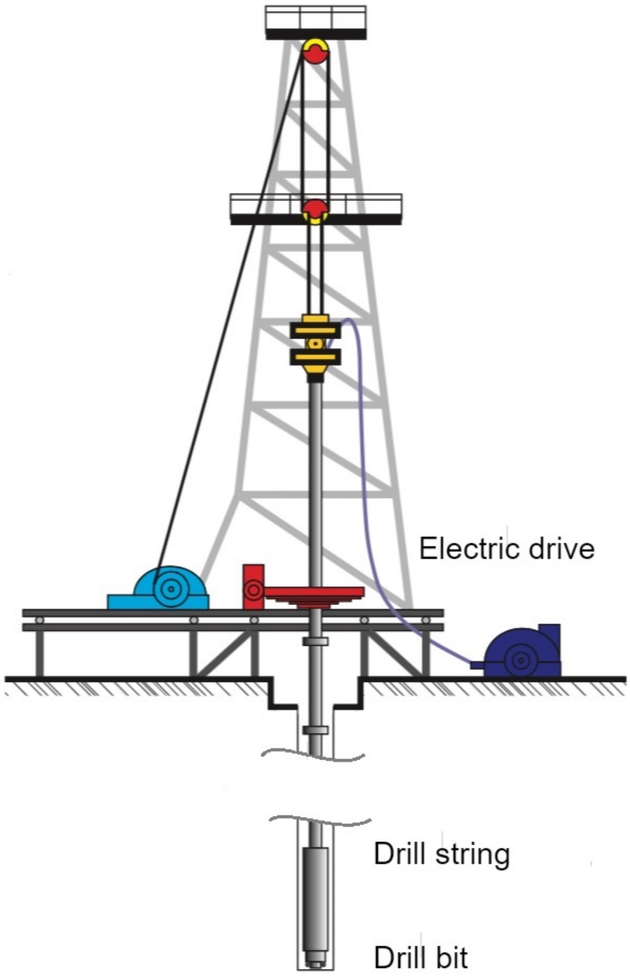

Figure 1.2: Typical drilling rig schematics with the most important components (adapted from [6]).

torsional vibrations and the stick-slip phenomenon.

The drill string is a long and slender structure, resulting in torsional vibration being a common occurrence. Torsional vibration involves the twisting and untwisting of the drill string due to nonlinear interactions with the rock formation. Stick-slip is a critical stage of torsional vibration, characterized by alternating stick and slip phases. During the stick phase, the drill bit halts while the top continues to rotate, storing elastic torsional energy. When the accumulated torque exceeds the friction torque, the slip phase occurs, leading to a sudden release of the drill bit and an acceleration to angular velocities significantly higher than the desired speed.

In addition to torsional vibrations, axial and lateral vibrations can also occur, leading to phenomena known as bit-bounce and whirling motion, respectively. These coupled phenomena increase the complexity of the system dynamics. Excessive drill string vibrations can result in reduced drilling efficiency and premature equipment damage.

Axial vibrations are particularly noticeable as they originate from the bottom of the well and propagate along the drill string to the surface. Bit-bounce occurs when the drill bit loses and regains contact with the rock surface, often caused by irregularities or axial resonances induced by the mud pump. While large axial vibrations can be detrimental to the process and equipment, controlled axial vibrations can have a positive effect under certain circumstances [7].

Although drilling and extraction techniques have improved, there is still room for enhancing the drilling process. This motivates more detailed studies on the dynamics of drilling systems, as oil companies seek to optimize drilling operations.

1.2 Objectives and contributions

The previous section provides a brief overview that highlights the significance of addressing oscillations in drilling systems. Based on this motivation, this thesis aims to investigate torsional and axial oscillations through the utilization of two laboratory-scale experimental test rigs. The primary goal is to develop a mathematical model for these nonlinear systems. In summary, the main objective of this thesis can be stated as follows:

1. Experimental analysis of lab-scale drill-string systems, providing insights into their behavior;

2. Development of mathematical models for torsional vibrations in slender systems, enhancing our understanding of their dynamics;

3. Implementation of system identification strategies for nonlinear systems, improving parameter estimation;

4. Experimental validation of the proposed identification methods, demonstrating their effectiveness.

This thesis makes significant contributions in several areas, including modeling torsional and coupled vibrations in drill-string systems, conducting comprehensive experimental tests under various conditions using a dedicated lab test rig for torsional oscillations, developing a novel configuration for a lab-scale drill-string system, experimentally validating the proposed dynamical models, and performing nonlinear analysis of the systems:

- Developing a low-dimensional torsional model based on an experimental setup to simulate the torsional behavior observed in real drilling systems. The dynamical model is then utilized to explore the influence of nonlinear control parameters on the dynamics of the system, utilizing both experimental and numerical data.
- Proposing an ensemble approach, which combines gray and black-box modeling techniques, to calibrate the parameters of a dynamical system, specifically those related to friction. The objective is to enhance the prediction accuracy compared to a pure gray-box approach while maintaining interpretability in the dynamic responses. To evaluate the effectiveness of the proposed method, four widely used friction models of varying complexity are employed. The analysis highlights that the ensemble of gray and black-box identification techniques yields superior results for friction modeling and simulation, offering an improved data-driven approach for constructing mathematical models of complex torsional dynamics in slender structures.
- Inferring the mechanical and friction parameters of a low-dimensional model using a neural network. The mathematical model is calibrated using experimental data obtained from a setup consisting of a DC motor and two rotating inertias connected by a slender shaft, where friction is introduced through braking on one of the inertias. The estimated parameters obtained from the neural network are then compared with the parameters identified through experimental measurements.
- Investigating the three types of vibrations observed during drilling, namely torsional and axial vibrations, using a specially developed lab-scale drilling rig. The primary focus of this investigation is to examine the coupling mechanism of these vibrations. A key contribution of this study is the detailed experimental analysis conducted using a vertical rig that incorporates real drill bits and rock samples. By utilizing this rig, the coupling mechanism of torsional and axial vibrations can be thoroughly examined, providing valuable insights into the dynamics of drilling operations.

These contributions collectively enhance our understanding of drill-string dynamics and provide valuable insights into the field.

Throughout the duration of the doctoral research, various articles were published in both journals and conferences, including:

- Ingrid Pires, Helon V. H. Ayala, and Hans I. Weber. *"Nonlinear ensemble gray and black-box system identification of friction induced vibrations in* *slender rotating structures"* Mechanical Systems and Signal Processing, 2023, 186, 109815.

- Ingrid Pires, Helon V. H. Ayala, and Hans I. Weber. *"Data-driven Model for Torsional Oscillations in Slender Structures"* XIX DINAME. Pirenopolis, Brazil, 2023.
- Ingrid Pires, Helon V. H. Ayala, and Hans I. Weber. *"Ensemble Models for Identification of Nonlinear Systems with Stick-Slip"* 10^{th} European Nonlinear Dynamics Conference. Lyon, France, 2022.
- Ingrid Pires, Helon V. H. Ayala, and Hans I. Weber. *"Nonlinear System Identification of an Experimental Drill-String Setup"* 16^{th} International Conference, Dynamical Systems - Theory and Applications. Lodz, Poland, 2021.
- Ingrid Pires, and Hans I. Weber. *"Stick-Slip Phenomenon: Experimental and Numerical Studies"* XV International Conference on Vibration Engineering and Technology of Machinery. Curitiba, Brazil, 2019.
- Ingrid Pires, Bruno C. Cayres, and Hans I. Weber. *"Nonlinear Dynamic Analysis of Torsional Friction-Induced Vibrations on Slender Structures"* 25^{th} ABCM International Congress of Mechanical Engineering. Uberlândia, Brazil, 2019.
- Ingrid Pires, Bruno C. Cayres, Djenane C. Pamplona, and Hans I. Weber. *"Torsional Friction-Induced Vibrations in Slender Rotating Structures"*XV IFToMM World Congress. Krakow, Poland, 2019.

1.3 Outline

Chapter 2 details the experimental test rig designed at the Dynamic and Vibration Laboratory of Pontifícia Universidade Católica do Rio de Janeiro. It introduces the key components of the test rig, encompassing sensors, and offers an operational overview. Additionally, the chapter presents the mathematical model utilized in the analysis for this dissertation, along with a compilation of the mechanical and electrical parameter values associated with the test rig.

Chapters 3, 4, and 5 are structured as self-contained research papers, allowing them to be read independently. Consequently, there may be some overlap between these chapters due to their standalone nature.

In Chapter 3, the torsional behavior of the experimental system at PUC Rio is examined, with a focus on investigating the influence of nonlinear control parameters on the system's response. Bifurcation diagrams are utilized, employing both experimental and numerical approaches, to analyze the system's behavior. The chapter introduces the dynamical model that was developed in a previous study [8], describes the experimental setup employed to simulate drill string oscillations, presents the results of numerical and experimental studies, and provides a comprehensive comparison between them.

Chapters 4 and 5 focus on the parameter estimation of a dynamical model for an experimental drill string setup using time-domain data. The test rig utilized in these chapters incorporates dry friction contact to emulate the nonlinear drill-bit interaction observed in actual drilling processes and dry friction models are employed in the mathematical model. In Chapter 3, a gray-box approach is proposed, and it is combined with a black-box technique in ensemble models. This combination aims to enhance prediction accuracy while preserving interpretability, as interpretability is crucial in solving real-world problems. Given the limitations of interpretability in some black-box methods, the use of a combined approach was chosen. In Chapter 4, a deep learning approach is introduced to estimate the same parameters discussed in the previous chapter, and the estimated parameters are compared with those determined experimentally.

Chapter 6 introduces the redesigned experimental drill-string system at the University of Aberdeen. The modifications made to the system allow for practical exploration of the coupling between axial and torsional oscillations, as well as the examination of specific parameters' influence on the phenomena of interest. The key enhancement in the system involves incorporating a contact region along the shaft, simulating the interactions between the drill string and borehole walls. This modification enables a more comprehensive investigation of the dynamic behavior and interactions within the drill string system.

Chapter 7 concludes the thesis by summarizing the findings and providing recommendations for future research directions.

2
PUC-Rio experimental setup

2.1
Introduction

This chapter describes the experimental test rig developed at the Dynamic and Vibration Laboratory of Pontifícia Universidade Católica do Rio de Janeiro. The design of the experimental system aimed at simulating the dynamics of an oil-field drill-string system, specifically focusing on torsional vibrations occurring at certain drilling depths. The creation and utilization of this experimental drill-string system offer an enhanced comprehension of the dynamic processes involved during drilling operations. The subsequent sections introduce the primary components of the test rig, including sensors, and provide an operational description. Furthermore, the mathematical model adopted in this dissertation's analysis is presented, followed by a listing of the mechanical and electrical parameter values of the test rig. Furthermore, the experimental findings from this system are leveraged in subsequent chapters (Chapters 3, 4, and 5)

2.2
The experimental drill-string setup

Replicating the torsional dynamics via laboratory tests permits their analysis in controllable conditions. The experimental setup employed in this study was developed at the Dynamics and Vibrations Laboratory of Pontifícia Universidade Católica do Rio de Janeiro. The test rig can replicate the undesired torsional oscillations observed during drilling processes, such as the stick-slip phenomenon, but it does not represent any particular system. The slender structure, designed to isolate the torsional mode from the other vibration modes, provides a way to investigate the dynamical response associated with the drilling process. Figure 2.1 presents a photograph, while Fig. 2.2 illustrates the schematics of the experimental setup, providing an overview of its main components.

The rig consists of a horizontal apparatus composed of a DC motor, a planetary gearbox with a reduction ratio of 8:1 coupled to the DC motor,

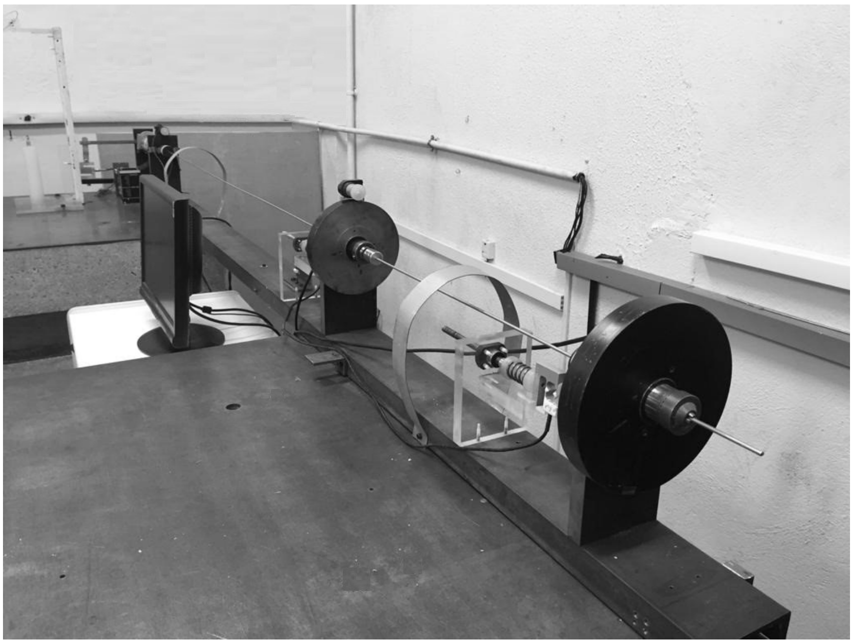

Figure 2.1: Experimental test rig.

two solid discs, and a low torsional stiffness shaft that transmits the rotation from the DC motor to the discs. The discs are free to rotate, and bearings constrain their lateral motion. A pin passing through the bearing support that comes in contact with the disc is used as a braking device to induce friction torque in the system. Due to this friction, the system experiences torsional vibrations resulting in stick-slip. The brake device does not correspond to the bit-rock interaction mechanism; its sole purpose is to introduce a resistive torque within the system. This torque allows the replication of the torsional oscillations commonly observed in drilling systems.

This study narrows its focus to the analysis of a specific system, encompassing the motor, intermediary disc, and the connecting shaft within the test rig. This deliberate choice allows for a systematic and phased approach to analyze the system. The shaft measures 1.7 meters in length with a diameter of 3 millimeters. Additionally, the inertial disc, connected to the shaft using a mandrel, possesses a thickness of 27 millimeters and a radius of 91 millimeters.

The motor and disc are equipped with LS Mecapion H40-8-1000VL encoders. The encoders are of optical quadrature type and have a resolution of 1000 ticks per revolution. The angular velocities of the inertia are calculated by numerical differentiation of the angular positions measured by the encoders. SV50 R-5 load cells from Alpha Instrumentos measure the normal force on the disc and the motor torque. We use a National Instruments cDAQ- 9174 as a real-time data acquisition platform.

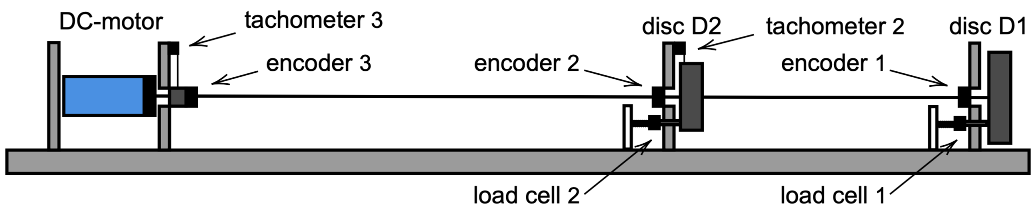

Figure 2.2: Schematic diagram of the experimental rig.

2.3 Dynamical Model

The authors derived a three degrees-of-freedom dynamical model in [8]. The mathematical representation depicted in Fig. 2.3 simplifies the mechanical subsystem as a torsional pendulum, which, despite its simplicity, effectively captures the stick-slip phenomenon. The mechanical subsystem comprises disc D2 and the shaft that links it to the DC motor. Disc D2 is characterized by a moment of inertia denoted as J_2. The torsional stiffness of the shaft is indicated by k_2, and the linear damping is represented by d_2. Conversely, the electric subsystem is depicted as a voltage source connected in series with a resistor and an inductor. Thus, the governing differential equations for the model presented in Fig. 2.3 are given by (2-1) [8].

In Fig. 2.3, τ_m represents the torque exerted on the shaft by the motor,

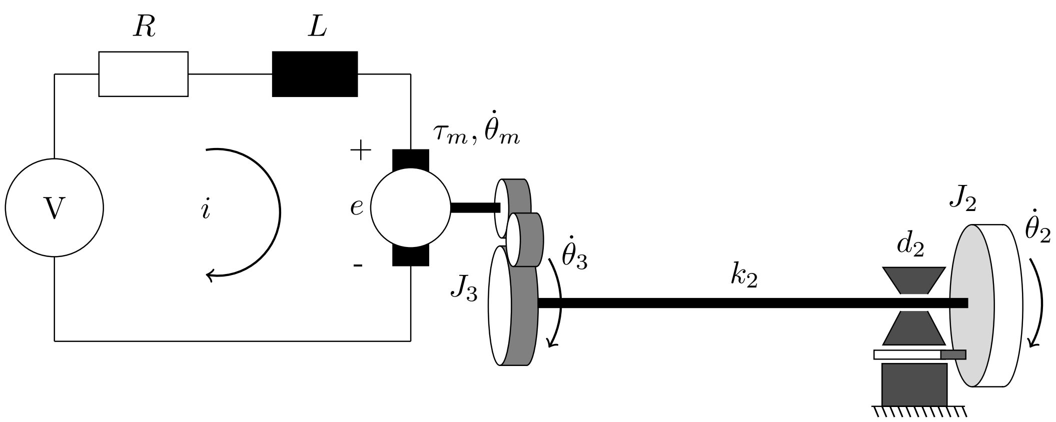

Figure 2.3: Diagram depicting the experimental arrangement featuring a DC motor, intermediary disc, and shaft. [8].

often referred to as motor torque. This torque is measured using a load cell.

$$\begin{aligned} J_2\ddot{\theta}_2 + d_2(\dot{\theta}_2 - \dot{\theta}_3) + k_2(\theta_2 - \theta_3) &= -T_{f2}, \\ d_2(\dot{\theta}_3 - \dot{\theta}_2) + k_2(\theta_3 - \theta_2) &= \eta(K_T i - C_m\eta\dot{\theta}_3 - T_f - J_m\eta\ddot{\theta}_3), \\ L\frac{di}{dt} + Ri + K_E\eta\dot{\theta}_3 &= V, \end{aligned} \tag{2-1}$$

here θ_2, $\dot{\theta}_2$, and $\ddot{\theta}_2$ are angular displacement, angular velocity and angular acceleration of D2, respectively, and T_{f2} is the resistive friction torque on disc D2. In (2-1), i denotes the DC-motor electric current, and L and R are the armature inductance and resistance, respectively. The angular velocity $\dot{\theta}_m$ is the velocity of the DC-motor inertia, J_m. C_m is the speed regulation; K_T, the constant motor torque; K_E, the voltage constant; and T_f, the internal friction torque. The transmission factor, η , is 8 : 1. The input voltage is $V = \kappa_p(\omega_{ref} - \dot{\theta}_3) + \kappa_i \int_0^t (\omega_{ref} - \dot{\theta}_3)dt$,where κ_p and κ_i are proportional constant and integral constant, respectively, and ω_{ref} is the reference velocity of the system.

(2-1) constitutes a set of three coupled differential equations, along with the nonlinearity associated with the friction torque. The resistive friction torque, T_{f2}, is explained in detail in [8].

In this thesis, the shaft is represented as a single torsional spring. This choice stems from prior analyses that employed continuum models and more degrees of freedom in modeling. The outcomes of these analyses indicated that a low-degree-of-freedom model sufficed for the objectives of this study.

2.4 Test Rig Parameters

This section lists the mechanical parameters identified in [71] alongside the cataloged electrical parameters. Table 2.1 presents the mechanical parameters of the system.

Table 2.1: Mechanical parameters of the test rig

Parameter	Value	Unit
J_2	149	kgm^2 (10^{-4})
k_2	0.3482	Nm/rad
d_2	0.0022	Ns/m

The electrical parameters, sourced from the manufacturer datasheet [50], can be found in Table 2.2. As these parameters have been retrieved from the motor catalog without independent identification, it is not possible to ensure their accuracy.

Table 2.2: DC-motor electrical parameters

Parameter	Value	Unit
L	$8.437(10^{-4})$	H
R	0.33	Ω
K_T	0.126	Nm/A
K_E	0.0602	V/(rad/s)
T_f	0.1196	Nm
C_m	$1.784(10^{-4})$	Nm/(rad/s)
κ_p	2.800	-
κ_i	3.500	-

2.5 Conclusion

In summary, this chapter thoroughly explores the PUC-Rio experimental system, designed to replicate the dynamics of a drill-string system in an oil-field setting, particularly emphasizing torsional vibrations encountered at specific drilling depths. The application of this experimental setup contributes to a heightened understanding of the intricate dynamics at play throughout drilling operations. The chapter introduces key components such as the test rig, dynamical model, and system parameters, some of which find application and relevance in the subsequent chapters.

3
Stick-Slip Phenomenon: Experimental and Numerical Studies

The stick-slip phenomenon is the most severe stage of the torsional oscillations present in most drilling routines. It results in drilling operations' inefficiency and damages the drilling equipment. Stick-slip arises from the strong nonlinear interaction between drill strings and borehole formation. This chapter delves into the analysis of torsional oscillations observed in slender structures such as drill strings. It utilizes the experimental configuration detailed in the preceding chapter, capable of emulating the torsional behavior witnessed in actual drilling systems. It proceeds to analyze the effect of nonlinear control parameters on the system dynamics by utilizing the experimental data collected.

It utilizes the experimental setup described in the previous chapter. The setup is capable of reproducing the torsional behavior experienced by real drilling systems. Finally, this chapter investigates the influence of the nonlinear control parameters in the system dynamics employing the experimental data collected.

3.1
Introduction

The excessive vibration of the drilling system leads to drilling operations inefficiency and damages the drilling equipment. Therefore, a good understanding of the system dynamics under different system conditions is necessary. The literature addressing drill string dynamics and experimental studies is vast [9, 10, 11].

Ideally, the entire drilling system should rotate at a constant speed. Although, due to the drill string's slenderness, torsional vibration is present in most drilling operations. The stick-slip phenomenon is the critical stage of torsional vibrations when the nonlinear interactions cause a complete arrest of the drill bit until it is suddenly released. Other modes of vibration are present during drilling as axial and lateral oscillations. The uncoupling of these three modes of vibration is considered in some studies as a simplifying hypothesis.

This chapter is centered on analyzing torsional vibrations. The research employs a purpose-built test rig to emulate torsional behavior akin to actual drilling systems. The experimental rig incorporates uncomplicated brake devices to introduce friction into the system, disrupting the rotational motion. By varying different combinations of parameters, the rig enables the experimental observation of diverse torsional responses.

This work aims to analyze the torsional behavior of the experimental system, investigating the influence of the nonlinear control parameters in the type of system response. For this purpose, experimental bifurcation diagrams are used.

3.2
Experimental Results

The drilling process is significantly influenced by a multitude of parameters, among which Weigh On Bit (WOB) and rotary speed play pivotal roles [5]. Hence, it is imperative to conduct experiments on a rig that operates under varying conditions, allowing a comprehensive exploration of how changes in parameters affect the system's response. In our experimental trials, we possess the capability to adjust either the normal force between the brake device and the pin or the reference velocity set by the DC motor.

As highlighted in the preceding chapter, our experimental setup incorporates diverse sensors to measure crucial parameters and variables about the system's dynamics. These sensors consist of three rotary encoders for tracking motor and disc speeds, as well as two load cells to gauge the normal force exerted by the brake devices. The experimental study covers various system parameters, including reference velocity and normal force. The experiments are carried out and documented with precision. To enable real-time monitoring and data preservation for later analysis, a LabVIEW-based Data Acquisition System (DAQ) is employed.

Figure 3.1 displays an example of time histories of a test for a certain combination of parameters where the existence of torsional vibrations with the stick-slip phenomenon is evident. The rig is driven from the motor with an angular reference velocity of 55 RPM, and the normal contact force applied to the disc is equal to 50 N.

Graphs (a) and (b) in Fig. 3.1 depict the friction torque and the normal contact force. In graph (c), it is possible to observe the oscillation of the disc's angular velocity. The normal contact force and angular velocity are measured as explained in the previous chapter, and the friction torque on the disc is calculated indirectly by utilizing the simplified mathematical model of the rig, as presented in (2-1). From the graph in (c), one may observe oscillations with a peak-to-peak amplitude of 110 RPM, which is twice the reference value.

As expected, a decrease in the friction torque with increasing speed and an increase with decreasing speed is noticed, aligning with findings in [13].

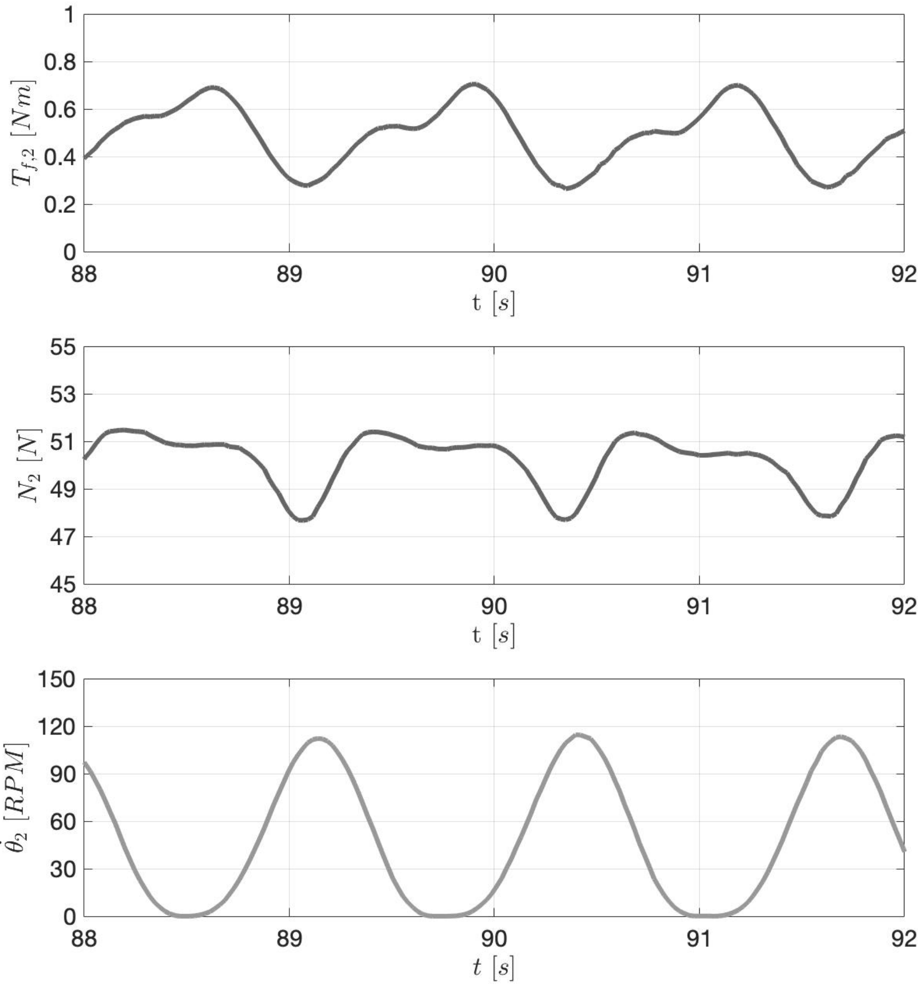

Figure 3.1: Torsional oscillations occurring in the reduced experimental rig for $\omega_{ref} = 55\ RPM$ and $N_2 = 50\ N$.

It's noteworthy that the normal force exhibits variations throughout the conducted tests. This phenomenon is due to the presence of ball bearings that support the disc, resulting in a slight deviation between the disc and the plane orthogonal to the shaft. In simpler terms, the disc rotates slightly out of the plane of contact between the disc and the pin, causing fluctuations in the magnitude of the normal force.

3.3 Nonlinear Analysis

As mentioned earlier, the test rig's dynamic behaviors can vary based on its parameters, mirroring the diversity seen in actual drilling systems. This section focuses on studying the experimental torsional vibrations observed in the rig, specifically emphasizing the stick-slip phenomenon. This critical phase of torsional oscillations manifests under various system conditions. To clarify, various combinations of the control parameters (specifically, normal contact force denoted as N_2 and reference angular velocity denoted as ω_{ref}) were explored. Additionally, the system demonstrates distinct stick-slip responses contingent on the combination of these control parameters.

To generate a bifurcation diagram, the mean value of the reference angular velocity was systematically adjusted, ranging from 5 to 55 RPM in increments of 2.5 N. This was done while maintaining a mean value of the normal force exerted by the braking device of 10N, allowing us to observe its impact on the dynamics of the rig. Figure 3.2 showcases the experimental bifurcation diagram. The plot includes the maximum and minimum values of angular velocity during the occurrence of the stick-slip phenomenon, and the mean value of angular velocity when the stick-slip phenomenon is absent.

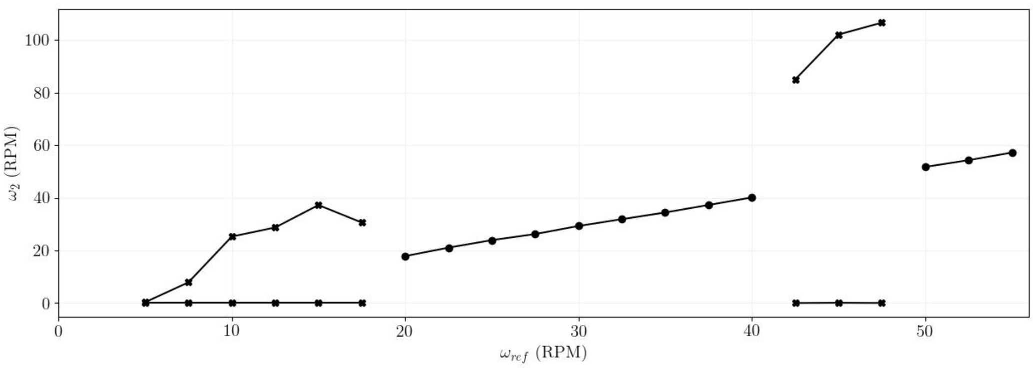

Figure 3.2: Bifurcation diagram with respect to reference angular velocity, ω_{ref}, for $N_2 = 10\ N$.

Examining the bifurcation diagram illustrated in Fig. 3.2, it is apparent that with an increase in ω_{ref}, the amplitudes of stick-slip oscillations also increase until they disappear, leaving only observable torsional oscillations. However, the experimental results reveal regions where stick-slip and oscillatory solutions interchange.

In Fig. 3.2 one may notice that the stick-slip phenomenon happens for values of ω_{ref} until 17.5 RPM and between 42.5 and 47.5 RPM. The system responses shown in Fig. 3.2 were obtained for a constant value of the normal contact force between the brake device and disc D2, $N_2 = 10$ N. The conclusion drawn from Fig. 3.2 is that the stick-slip phenomenon diminishes as ω_{ref} increases.

Similarly, an analogous analysis was carried out to observe how the system's response is affected by the normal force, N_2. The normal force, N_2, was systematically varied from 0 to 50 N in 2.5 N increments while keeping $\omega_{ref} = 55$ RPM constant. As observed in the previous section, the nature of N_2 varied during the tests (Fig. 3.1). However, for the sake of simplicity, we assumed it to remain constant in this analysis. Figure 3.3 showcases the experimental bifurcation diagrams concerning N_2.

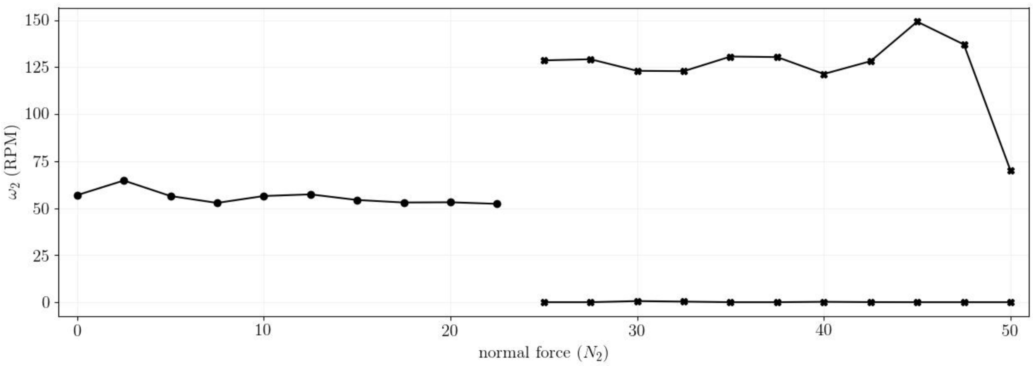

Figure 3.3: Bifurcation diagram with respect to normal contact force, N_2, for $\omega_{ref} = 55\ RPM$.

From Fig. 3.3, one may notice that for the lower values of N_2, there are torsional oscillations. As N_2 increases so do the amplitudes of torsional oscillations, and the stick-slip phenomenon appears.

3.4 Concluding Remarks

In this study, a brief analysis of the torsional dynamics exhibited by an experimental rig was conducted. The test rig, developed at Pontif'icia Universidade Cat'olica do Rio de Janeiro, accurately replicates the torsional behavior observed in real drilling systems. The primary objective of this analysis was to determine the conditions under which the stick-slip phenomenon is most likely to manifest. Our findings indicate that the stick-slip phenomenon tends to occur at lower reference velocity values and higher normal contact force values. Moving forward, our future research will focus on devising new predictive control methods to mitigate and suppress the stick-slip phenomenon.

4
Nonlinear Ensemble Gray and Black-box System Identification of Friction Induced Vibrations in Slender Rotating Structures

Due to the nonlinear bit-rock and drill-string-borehole interactions, the modeling and analysis of drill string dynamics are challenging work. These slender structures are subjected to torsional, lateral, and axial vibration modes, which are generally prejudicial to the drilling process. For this reason, proper mathematical modeling of the system dynamics is necessary to optimize drilling performance. This chapter focuses on the torsional dynamics and modeling of an experimental system subjected to friction torque. An ensemble approach, combining gray and black-box modeling techniques, is used to calibrate some of the dynamical system parameters, particularly those related to friction. This combination is chosen with the aim of improving the prediction accuracy of a pure gray-box approach while retaining physical interpretability in the dynamic responses. The present analysis compares four well-known friction models with increasing levels of complexity using experimental data. It is shown that the ensemble model proposed can improve the gray-box by up to 92.68% in terms of prediction errors, by adding a non-physical layer to it. This analysis demonstrates that better results can be obtained by using an ensemble of gray and black-box identification techniques for friction modeling and simulation, aiming at improving data-driven model construction of complex torsional dynamics in slender structures.

4.1
Introduction

Drill string dynamics is a challenging problem in dynamical modeling and analysis. The drill string is the component of the drilling system responsible for transmitting torque and motion from the top drive to the drill bit. Due to the nonlinear bit-rock and drill-string-borehole interactions, these slender structures are subjected to torsional, lateral, and axial vibration modes [14]. Lately, the torsional vibrations related to the so-called stick-slip phenomenon have become the leading research interest topic in drilling dynamics [11].

Stick-slip is a friction-induced limit cycle. In drilling operations, stick-slip occurs when friction causes a halt of the drill bit (stick phase), while the top drive continues to rotate until the stored energy overcomes the friction torque, and the bit is set in motion (slip phase). Downhole measurements have proved that when subjected to stick-slip conditions, the rotational speed of the drill string changes from rest to more than 300 rev/min in just a fraction of a second [15]. Typically, friction-induced self-sustained vibrations, like stick-slip, adversely affect the performance of mechanical systems [16, 17]. Thus, representative mathematical descriptions are imperative to reduce or avoid these oscillations, as they enable analysis and simulation of such phenomena.

Many authors have addressed the topic of drill string dynamics and proposed a variety of mechanical models based on lumped parameters, the Cosserat continuum, and beam theory formulations [18, 19, 20, 21]. In lumped-parameter models, the most common approach to study torsional vibrations is to assume that the system behaves as a torsional pendulum [22] and that the nonlinear interactions follow a velocity-dependent dry friction law [19]. Xie et al. [23] studied the dynamic behavior of a drill string in a horizontal well with a six-degrees-of-freedom model, considering a state-dependent time delay to account for the cutting process. The drill string vibrations were extensively investigated through experimental studies. In [9], the authors review some of the experimental rigs developed to examine drill string vibrations. Liu et al. [24] analyzed the multistability of drill strings by applying a small-scale downhole drilling rig and performed a parametric study of the stick-slip phenomenon. Real et al. [25] proposed a model with hysteresis for the bit-rock interaction based on laboratory test rig data.

The nonlinear interaction modeling plays an essential part in the research associated with drilling dynamics. A usual approach considers the dependence of the forces and torque on the bit speed through dry friction. Regarding the stick-slip behavior, the complexity of the investigation lies in the fact that static friction governs the motion during the stick phase, while velocity-dependent kinetic friction rules govern them during the slip phase [16]. In their paper, Silveira and Wiercigroch [26] numerically investigated the influence of friction complexity on the dynamical responses of the system. The complicated friction interactions were addressed by Hasnijeh et al. [27] using stochastic interpretation. Riane et al. [28] cited the lack of measurement devices to accurately measure bottom torque as the major problem in modeling the rock-bit interaction and overcoming this situation by estimating the unknown torque with a Kalman filter. The authors of [28] also modeled the nonlinear dynamics of the downhole using a proportional-integral observer in [29]. Bit-rock and wellbore interactions, eccentricity, and hydrodynamic forces due to fluid resistance to lateral bending were taken into account in the investigation of Moraes, and Savi [30]. The authors worked with a four-degree-of-freedom nonsmooth model with axial-torsional-lateral vibration coupling.

Mathematical modeling is the first step to consider in studying system dynamics. Notwithstanding the number of existing numerical and experimental investigations in the dynamics of slender systems, like drill strings, most of the mathematical models available were developed analytically. Practical limitations of analytical analysis motivate the application of system identification, which comprises a set of techniques for building data-based models. Concerning system identification, Aguirre [31] says there are three types of identification techniques, distinguished by the amount of prior knowledge. These are the white-box approach, specified by prior knowledge and physical insight; the gray-box approach, obtained from less physical insight (physical and semi-physical models); and the black-box approach, constructed in the absence of a priori knowledge. In the context of dynamical systems with friction identification, there are contributions published in [32, 33, 34, 35, 36, 37]. Janot et al. [33] proposed a state-dependent-parameter method of nonlinear estimation as an alternative to the standard inverse dynamical identification model with the least-squares technique. The authors evaluated the performance of the proposed approach on two dynamic systems. One of them is the electromechanical positioning system (EMPS) detailed in [34]. In Auriol et al. [37], the authors compare three methods to estimate the friction parameters that describe the nonlinear drill-string-borehole interactions. The authors of [35] modeled the same EMPS with a combination of gray and black-box approaches. The authors claim that the hybrid formulation performs better than the gray box alone. In [32], Worden et al. modeled the friction dependence on displacement and velocity using physics-based and black-box approaches. They compared their modeled and experimental force time-series data. Their models showed good prediction capability, and the ensemble models achieved the best results. In [38], the authors also discussed the application of gray and black-box techniques in ensemble models. They studied three benchmark problems, one of them being a Bouc-Wen Hysteretic System.

Despite the endeavor dedicated to the analysis and modeling of drill string dynamics, there is no consensus on a model that is considered to be comprehensive [11]. Experimental investigations employing small-scale laboratory rigs have been a good approach. However, most of the mathematical models developed for the experimental setups of drilling rigs are developed applying analytical modeling and not measurements [9]. Regarding the construction of data-based models for friction systems, most of the related literature deals with systems where the stick-slip phenomenon is not present [32, 33, 38]. Moreover, the researchers usually utilize friction force data to calibrate their models.

This study uses time-domain data to propose a dynamic model for an experimental drill string setup. The test rig used in this study employs dry friction contact to simulate the nonlinear drill-bit interaction present in drilling processes. Although most friction research focuses on phenomenological formulations, this chapter proposes the application of the gray-box approach and the combination with a black-box technique in ensemble models. This technique is adopted to increase the accuracy of the predictions without losing physical interpretability. As some black-box methods have limitations of interpretability, and solving real-world problems requires it, the option made in this work was a combination of approaches. As the intent is to use a dynamical model for prediction and analysis, it is expected to replicate the system's dynamic behavior and, at the same time, diminish the prediction errors. The main contribution of this work is that it explores the suitability of an ensemble of gray and black-box approaches for the identification of friction models, particularly with systems that exhibit the stick-slip phenomenon. Other contributions of this work are: (i) the model identification of the stick-slip phenomenon in a slender experimental system based on input and output data; (ii) the analysis of different friction models' capability of reproducing the phenomenological aspect; and (iii) the use of hybrid formulations for nonlinear system identification.

This chapter is organized as follows. Section 4.2 presents the theoretical background of this study, including friction models and system identification approaches. Section 4.3 briefly describes the model for the experimental setup and presents the experimental data employed in the investigation. Section 4.4 introduces the ensemble model proposed in this work. Section 4.5 evaluates the performance of the proposed methodology and discusses its numerical results. Finally, the conclusions are outlined in Section 4.6.

4.2 Theoretical Background

Many different dynamical models have been devised to study drill-string dynamics, and it has been observed that, among other factors, the accuracy of the simulations depends on the choice of a friction model and its calibration.

Adjusting the parameters of a friction model is not a simple endeavor. Among the many methods available to perform this task, the focus relies on studying and comparing a gray-box approach against an ensemble (mixed) one used to calibrate the parameters associated with friction, stiffness, and damping.

4.2.1 The Friction Models

Many mathematical formulations to describe dry friction have been developed over the years. For example, [39, 40] include a review of some of the most common models employed in dynamical systems. In this study four different friction formulations are considered to obtain the resistive torque T_f that will be used in the dynamical model of the test rig, these are:

- The regularized Coulomb friction model
- The regularized Stribeck friction model
- The Dahl friction model
- The Stefanski et al. friction model

The classical Coulomb friction model states that friction opposes the relative motion between contacting surfaces, and its magnitude is proportional to the normal contact force [41]. The following equation defines the unregularized model:

$$F_f = F_C \mathrm{sign}(v), \tag{4-1}$$

where F_f is the friction force, $F_C = \mu_k F_N$ is the magnitude of Coulomb friction, v is, from the perspective of the body, the relative tangential velocity between the contacting surfaces, F_N is the normal force, and μ_k is the kinetic friction coefficient. This model presents a velocity dependence by the sign function that introduces a discontinuity in the system of ODEs. Instead, this study considers a regularized approximation using the hyperbolic tangent with a transition velocity v_t to avoid discontinuities. Therefore, the regularized Coulomb friction is:

$$F_f = F_C \tanh\left(\frac{v}{v_t}\right). \tag{4-2}$$

Because of its simplicity, the regularized Coulomb model is very suitable for System Identification.

The second model employed was the Stribeck curve. Stribeck [42] proved that friction decreases as the relative velocity increases for low velocities. In a general form, the Stribeck curve is defined by some function $g(v)$, and the friction equation is:

$$F_f = (F_C + (F_S - F_C)g(v)\tanh\left(\frac{v}{v_t}\right) \tag{4-3}$$

Tustin [43] described $g(v)$ as:

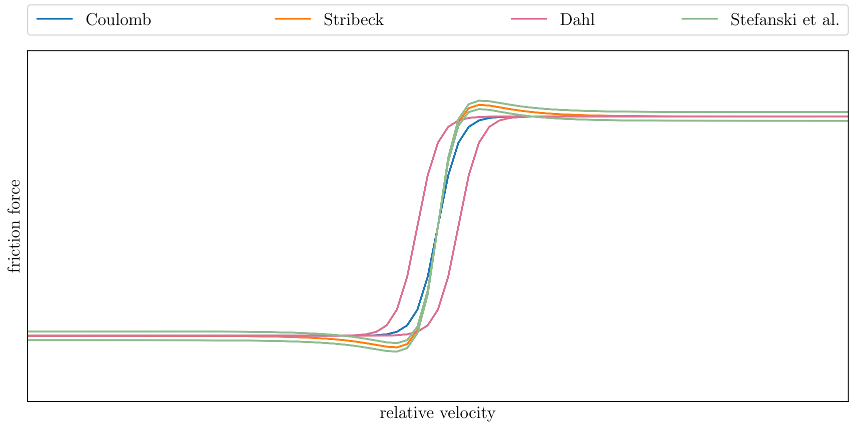

Figure 4.1: Comparison of friction models.

$$g(v) = exp\left(-\frac{|v|}{v_s}\right) \tag{4-4}$$

where v_s is the Stribeck velocity, a limit value of the relative velocity at which the friction behavior changes from boundary high friction at low velocity to lower friction at higher velocity [40].

The friction models mentioned above do not account for the hysteresis loops observed in reality. Therefore, two other friction models were also utilized: Dahl [44], and Stefanski et al. [45, 46, 40], to consider the hysteresis effect. The Dahl model characterizes the friction behavior in the pre-sliding stage by considering:

$$\dot{F}_f = \sigma_0\left(1 - \frac{v}{F_C}\right)\text{sign}(v)v, \tag{4-5}$$

where σ_0 is the stiffness coefficient.

The model proposed by Stefanski et al. (2003) [45] takes into consideration the dependence on both relative velocity and acceleration. This model defines the $g(v)$ function of (4-3) as:

$$g(v) = exp\left(-\frac{\alpha_1|v|}{|\dot{v}| + \alpha_2}\right)\text{sign}(v\dot{v}) \tag{4-6}$$

where α_1 and α_2 are constants. A summary of the four friction models, showing their shape and differences, is given in Fig. 4.1.

4.2.2
Gray-box aproach

White, gray, and black-box approaches differ in the amount of theoretical knowledge. While the white-box models are entirely theoretical and the black-box, experimental, gray-box models combine the benefits of both [47]. Physical or semi-physical models are special cases of gray-box modeling and deal with estimating the physical parameters of a system. The parameter estimation problem, in this work, is framed as an optimization problem with the objective/cost function defined as a mean-square error between experimental data and predictions:

$$C(\beta) = \frac{1}{N}\sum_{i=1}^{N}(y_i - y_i(\hat{\beta}))^2. \tag{4-7}$$

C is the cost function to be minimized. y_i and $\hat{y}_i$ are the experimental and predicted data, respectively. The unknown parameters vector is named β.

4.2.3 Black-box approach

The black-box approach is constructed in the absence of a priori information. Data acquired from experimentation is used to capture the system dynamics in this modeling. Regarding Black-box, the AutoRegressive eXogenous (ARX) model was employed. The error was modeled using the ARX structure [31]:

$$\begin{aligned} y(k) &= +A_1 y(k-1) ... + A_{n_y} y(k-n_y) \\ &+B_1 u(k-1) ... + B_{n_u} u(k-n_u) + \varepsilon(k), \end{aligned} \tag{4-8}$$

where $y(k)$, $u(k)$ are the system output and input, respectively; $\varepsilon(k)$ is the model error at instant k; A and B are linear estimators matrices; and n_y and n_u are the maximum lags at the system output and input, respectively.

4.3 The experimental system

The setup detailed in Chapter 2 is utilized for this study.

4.3.1 The system dynamical model

The system dynamics is modeled by assuming that the experimental rig presented in Chapter 2 behaves as a torsional pendulum. It was assumed that the only resistive torque in the system was caused by the friction torque induced by the braking device. The mechanical subsystem, composed of one of the discs and the shaft connecting it to the DC motor, is modeled as:

$$\begin{aligned} J_d\ddot{\theta}_d + c(\dot{\theta}_d - \dot{\theta}_m) + c_d\dot{\theta}_d + k(\theta_d - \theta_m) &= -T_f, \\ J_m\ddot{\theta}_m + c(\dot{\theta}_m - \dot{\theta}_d) + c_m\dot{\theta}_m + k(\theta_m - \theta_d) &= \tau_m, \end{aligned} \tag{4-9}$$

where θ, $\dot{\theta}$, and $\ddot{\theta}$ are the angular displacement, angular velocity, and angular acceleration of the two inertias, respectively. J_d and J_m are the moments of inertia of the disc and the DC motor. The shaft stiffness is denoted by k, and internal damping is denoted by c. The external dampings are c_d and c_m. T_f is the resistive friction torque on disc D2, and τ_m is the torque transmitted to the mechanical subsystem.

The resistive friction torque T_f, required for the dynamical system model, is given by:

$$T_f = F_f a, \tag{4-10}$$

where a is the distance between the disc center and the disc-pin contact area. For simplicity, $T_C = F_C a$ is considered the resistive torque related to the kinetic Coulomb friction, and $T_S = F_S a$ is the one related to the static friction.

The electric subsystem is composed of a voltage source connected in series with a resistor and an inductor, providing torque τ_m. The angular velocity imposed by τ_m is eight times greater than the angular velocity $\dot{\theta}_m$ transmitted to the mechanical subsystem due to the transmission factor $\eta = 8:1$. Mathematically, the electric subsystem can be expressed as:

$$\begin{aligned} L\frac{di}{dt} + Ri + \eta K_E \dot{\theta}_m &= V, \\ \tau_m &= \eta(K_T i - T_{fm}), \end{aligned} \tag{4-11}$$

where i denotes DC-motor electric current. L and R are the armature inductance and resistance, respectively. K_T is the constant motor torque; K_E, the voltage constant; and T_{fm}, the internal friction torque. The input voltage is denoted by V and is given by

$$V = \kappa_p(\omega_{ref} - \dot{\theta}_m) + \kappa_i \int_0^t (\omega_{ref} - \dot{\theta}_m)dt, \tag{4-12}$$

where κ_p and κ_i are proportional constant and integral constant, respectively, and ω_{ref} is the reference velocity of the system.

In the present model and simulations, the electrical subsystem was disregarded. Instead, only the mechanical is considered, using the torque generated by the electric motor, τ_m as the input for the mechanical system.

To simulate (4-9) the following state-variables were defined:

$$\mathbf{X} = \begin{bmatrix} \delta & \dot{\theta}_d & \dot{\theta}_m \end{bmatrix}^T,$$

where $\delta = \theta_d - \theta_m$ is the angular difference. Therefore, (4-9) can be rewritten as a state-space system as follows:

$$\dot{\mathbf{X}} = \begin{bmatrix} 0 & 1 & -1 \\ -k/J_d & -(c+c_d)/J_d & c/J_d \\ k/J_m & c/J_m & -(c+c_m)/J_m \end{bmatrix} \begin{bmatrix} \delta \\ \dot{\theta}_d \\ \dot{\theta}_m \end{bmatrix} + \begin{bmatrix} 0 & 0 \\ -1/J_d & 0 \\ 0 & 1/J_m \end{bmatrix} \begin{bmatrix} T_f \\ \tau_m \end{bmatrix}$$

$$y_m = \begin{bmatrix} 0 & 1 & 0 \end{bmatrix} \begin{bmatrix} \delta \\ \dot{\theta}_d \\ \dot{\theta}_m \end{bmatrix}; \tag{4-13}$$

y_m is the output of our mathematical model.

4.3.2 Measured data

The measurements of forces, displacements, and velocities were conducted using a LabVIEW-based Data Acquisition System (DAQ). The sampling frequency during these measurements varied in a non-constant manner, ranging between 38.46 and 43.48 Hz. To standardize the data, the signals were resampled to a uniform frequency of 100 Hz through interpolation. Subsequently, the resampled data was processed using a low-pass Butterworth filter, a process carried out using Matlab.

The test rig is a closed-loop electromechanical system with an output motor velocity driven by a Proportional-Integral (PI) controller (4-12). The velocity set-point is called reference velocity. According to [49] closed-loop identification can be performed for consistent models or unmodelled dynamics.

The input trajectory was obtained by measuring the motor torque in the mechanical system, which is driven by the PI controller of the motor, described in (4-11) and (4-12). Figure 4.2 presents the time histories of an experiment: Fig. 4.2a depicts the time history of the disc angular velocity (system output) whereas Fig. 4.2b shows the time history of the motor torque, τ_m (system input). The disc angular velocity, ω_d, is derived through numerical differentiation of the angular position, which is measured using an encoder, and the motor torque, τ_m, is measured employing a load cell, as detailed in section 2.2. This result was acquired for a reference angular velocity of 5.76 rad/s and an average normal contact force between pin and disc of 50 N. This combination of values was selected because it induces stick-slip oscillations in the system, which is the condition of interest in this study. The signals were recorded for 270 seconds.

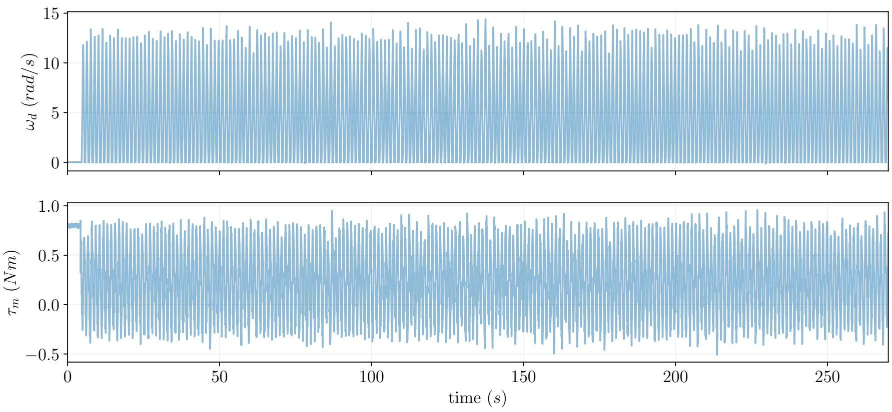

Figure 4.2: Measured time history of (a) disc angular velocity, ω_d; and (b) motor torque, τ_m.

4.4 The proposed methodology

This study aims to utilize the prior knowledge of the experimental test rig physical model to enhance the accuracy and to reproduce the stick-slip phenomenon by employing an ensemble model (a combination of a gray-box and a black-box component). Firstly, estimating the parameters of the physical model, and secondly, fitting a network to the residuals. In addition, the results will be compared to those obtained with a sole gray-box approach to determine if any improvement is achieved.

The methodology employed for the simulations considering the sole gray box is presented. After that, a description of the ensemble approach is provided.

As aforementioned, the first step of this work is the estimation of the mechanical parameters of the experimental system. At this point, a gray-box approach was developed by fitting a semi-physical model. To do so, it employed the measured input and output data of the time interval from 30 to 90 seconds of the recording in Fig. 4.2. The validation used the measured input and output data of the time interval from 120 to 180 seconds.

The interest of the present analysis is to estimate the mechanical parameters of the test rig, shaft stiffness and damping, and friction parameters. Although certain parameters have been determined through experimental analysis, this study involves their estimation as a fundamental aspect of the proposed methodology. These specific parameters of interest are collectively represented by the vector β as follows:

$$\beta_1 = \begin{bmatrix} k & c & c_d & c_m & T_C \end{bmatrix}, \qquad \beta_2 = \begin{bmatrix} k & c & c_d & c_m & T_C & T_S & V_S \end{bmatrix},$$
$$\beta_3 = \begin{bmatrix} k & c & c_d & c_m & T_C & \sigma_0 \end{bmatrix}, \quad \beta_4 = \begin{bmatrix} k & c & c_d & c_m & T_C & T_S & \alpha_1 & \alpha_2 \end{bmatrix},$$

subscripts 1, 2, 3, and 4 correspond to the optimization problems with the four friction models: Coulomb, Stribeck, Dahl, and Stefanski et al., respectively. For the optimization problem, lower and upper bounds for the unknown parameters were defined by physical restrictions.

The disc inertia was obtained straightforwardly by direct measurement, and the motor inertia from its manual [50]. The values are $J_d = 0.0149\ kgm^2$ and $J_m = 0.0234\ kgm^2$.

To solve this nonlinear optimization problem, this work applied the CasADi [51] interface to Interior-Point OPTimzer (IPOPT) [52]. CasADi is a symbolic framework for numerical optimization. In this framework, solving an optimization problem consists of the symbolic representation of the problem construction and the minimization of the objective function (5-5) with IPOPT. The IPOPT open-source code is a widespread implementation of an Interior-Point method.

The second step was to build a black-box model of the error between the measurements and the estimations obtained from the gray-box approach.

The author simulated the system for each one of the friction models selected with the set of estimated parameters obtained from the minimization of the cost function in (5-5) and calculated the error between estimation and measured data. Then, a toolbox in Matlab was used to determine the black-box model parameters of the error. This work used 60 seconds of motor torque and disc angular velocity data for system identification and 60 seconds to validate the identified models.

As aforementioned, it was intended to use both the prior knowledge of the physical model and the black-box component to enhance the accuracy of the predictions. According to [38], one way to do this is to use a white box as a mean function and fit the model residuals using a black-box algorithm. Instead, in this study, the gray-box model was used as a mean function and the residuals were modeled with a black-box algorithm in a difference equation:

$$y_e(k) = \overbrace{f(x(k), u(k))}^{\text{gray-box}} + \overbrace{g(e(k-1), ..., e(k-n_e), u(k-1), ..., u(k-n_u))}^{\text{black-box}} \tag{4-14}$$

where y_e is the output of the ensemble model. y_e is a sum of the system model output (4-13) and the model residual. $f(x(k), u(k))$ is a function of the system

Table 4.1: Estimated parameters values

	Coulomb	Stribeck	Dahl	Stefanski et al.
k (Nm/rad)	0.1614	0.1593	0.1534	0.1550
c (Ns/m)	0	0.0012	0	0
c_d (Ns/m)	0	0.0033	0.0035	0.0036
c_m (Ns/m)	0.0071	0.0175	0.0209	0.0205
T_C (Nm)	0.2278	0.1167	0.1203	0.1131
T_S (Nm)		0.4146		0.4120
V_S (rad/s)		0.1138		
σ_0			0.0149	
α_1				33.64
α_2				33.64

input u, and states x, and the residual is a function of the system input u and itself.

The general idea of the proposed method is to combine the physics-based approach and an ARX model to capture the response aspects missed by the physical model alone, improving the predictions.

4.5 Validation and discussion

This work evaluated the performance of the proposed identification methodology via simulation. First, it integrated the equations of motion (4-9) utilizing the solver ode45 from Matlab for each one of the friction models selected. The simulations employed the experimental data for input τ_m. The error was incorporated into the model as in (4-14). The data set employed for validation analyses is different from the one used for model identification and is composed of experimental data from 120 to 180 seconds.

4.5.1 Gray-box model

Table 5.1 gives the set of estimated parameters obtained from the minimization of the cost function in (5-5). This work performed the parameter estimation employing the system dynamics forward simulation. Using the estimated parameter depicted in Table 5.1 the system was simulated and the computed free-run predictions were compared with the experimental data in the validation time interval. Fig. 4.3 depicts the direct comparison of experimental and estimated time histories of the disc angular velocity for the validation set.

From Fig. 4.3, one may observe that there are differences in the amplitude of oscillation, whereas no differences in the vibration frequency are found. One

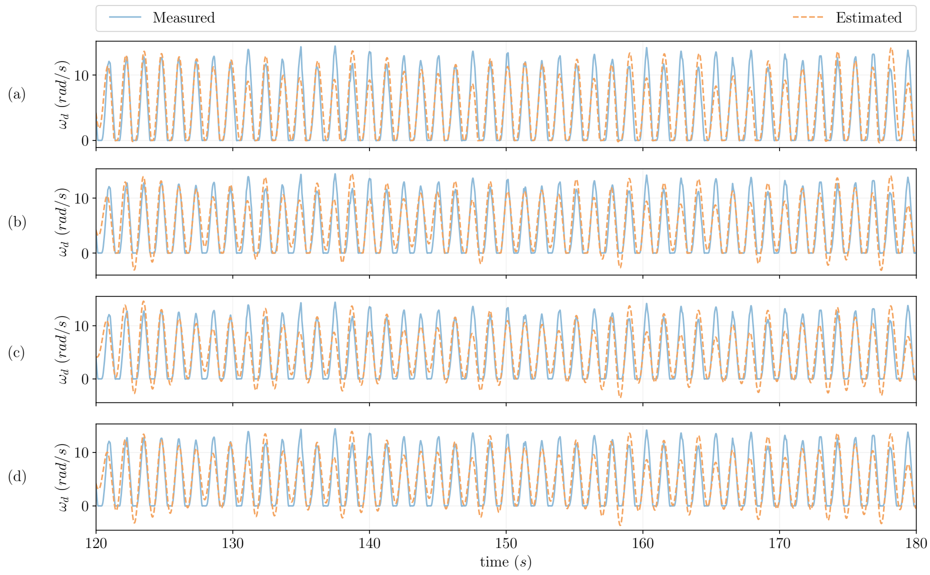

Figure 4.3: Comparison of measured and predicted disc angular velocity using gray-box model based on (4-9): (a) Coulomb (RMSE 2.0063); (b) Stribeck (RMSE 2.1110); (c) Dahl (RMSE 2.2558); (d) Stefanski et al. (RMSE 2.1462).

can observe that the disc angular velocity obtained from the mathematical model in Fig. 4.3a properly recovers measured data. While the three other models (Figs. 4.3b-d) result in responses with negative angular velocities. How well the models capture the friction phenomena - transitions from stick to slip and vice versa - determines the model's accuracy. To better observe this aspect, Fig. 4.4 shows one stick phase interval, comparing measurements and estimations for each one of the models. Figure 4.4 shows that three of the friction models fail to reproduce the stick-slip phenomenon.

4.5.2
Ensemble model

The ARX model with motor torque τ_m as input, and error e as output was built as follows:

$$e(k) = a_1 e(k-1) + a_2 e(k-2) + b_1 \tau_m(k-1) + b_2 \tau_m(k-2), \tag{4-15}$$

where a_1, a_2, b_1 and b_2 are the parameters of the ARX model. The black-box model was trained with the recorded input and output data of the time interval from 30 to 90 seconds of the recording in Fig. 4.2 and validated by employing the recorded input and output data of the time interval from 120 to 180 seconds. The choice of the mathematical model architecture (4-15) was motivated by the analysis of the prediction errors and the capability to

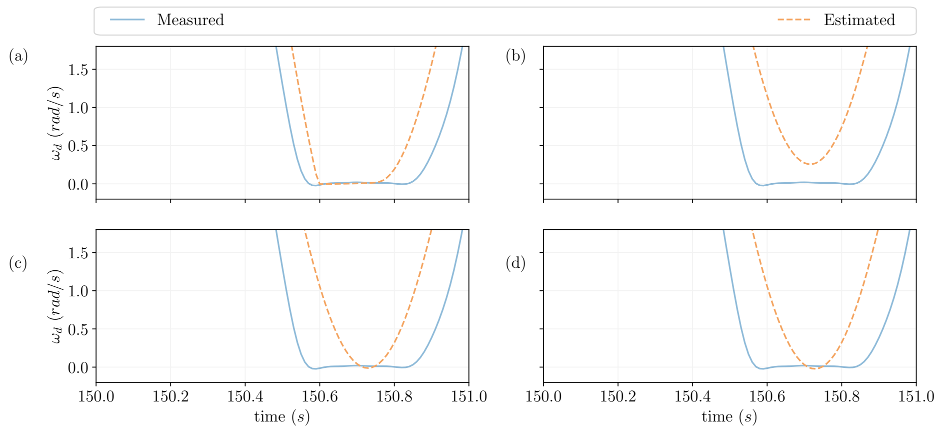

Figure 4.4: Comparison of measured and predicted disc angular velocity using gray-box model based on (4-9), one stick phase interval: (a) Coulomb; (b) Stribeck; (c) Dahl; (d) Stefanski et al.

Table 4.2: Mean stick duration for all four friction models tested

	Gray-box model	Ensemble model
Coulomb	0.2761	0.3662
Stribeck	0.1614	0.3628
Dahl	0.0701	0.3662
Stefanski et al.	0.0665	0.3677

reproduce stick intervals.

The ensemble model was constructed as displayed in (4-14). Fig. 4.5 depicts the accuracy of the free-run prediction obtained with this method, plotting the direct comparison of experimental and estimated time histories of the disc angular velocity for the validation set. All the ensemble model simulations are able to reproduce the experimental system dynamics, which means that one can observe torsional oscillations with the stick-slip phenomenon in all four outputs. It is possible to notice the same general dynamic response at this point when comparing the graphs of Fig. 4.5.

Fig. 4.6 shows one interval of the stick phase, comparing measurements and estimations for each one of the friction models. From Fig. 4.6 one may conclude that the ensemble model formulation was a far more effective model. In Table 4.2, the estimated mean stick duration for all models studied is presented. The mean stick interval duration calculated from experimental measurements equals 0.3770. Among gray-box models, Columb is the one with the closest value, as expected from the observation of Fig. 4.4. Concerning the model using the ensemble approach, the closest value was obtained by using the Stafansi et al. friction model. From Table 4.2, one can see significant differences in the values of mean stick interval duration obtained from the gray-box and the ensemble approaches for three of the four friction models tested.

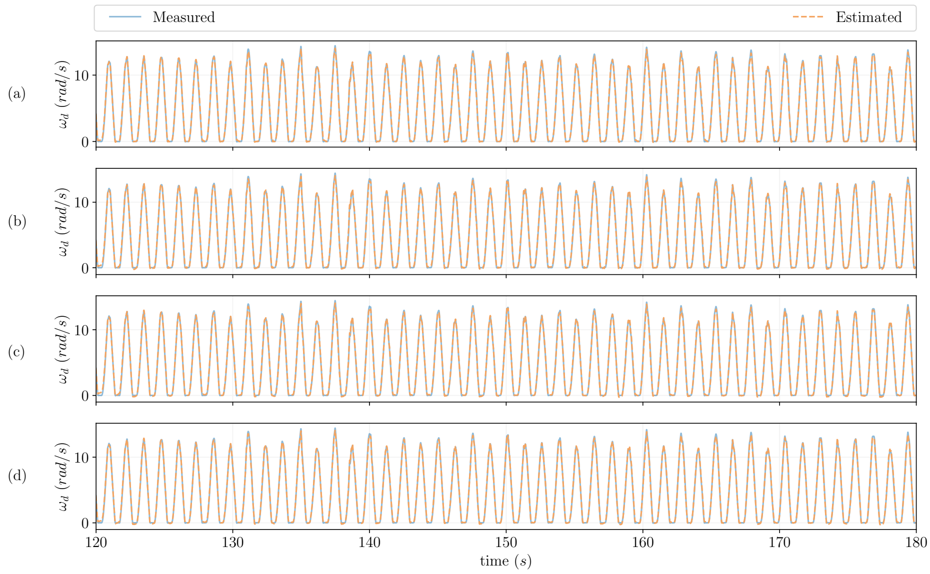

Figure 4.5: Comparison of measured and predicted disc angular velocity using ensemble model based on (4-9), (4-8) and (4-14): (a) Coulomb (RMSE 0.1697); (b) Stribeck (RMSE 0.1748); (c) Dahl (RMSE 0.1652); (d) Stefanski et al. (RMSE 0.1587).

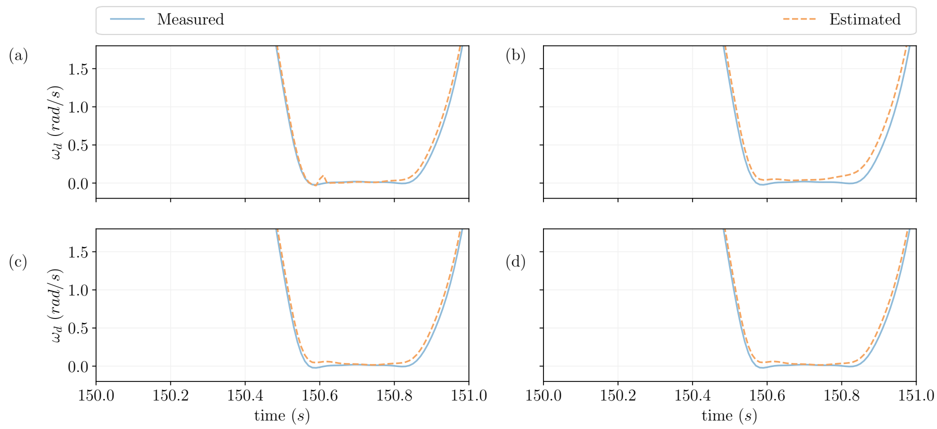

Figure 4.6: Comparison of measured and predicted disc angular velocity using ensemble model based on (4-9), (4-8) and (4-14), one stick phase interval: (a) Coulomb; (b) Stribeck; (c) Dahl; (d) Stefanski et al.

Table 4.3: RMSE and maximum error scores for all four friction models tested

	Gray-box model		Ensemble model		
	RMSE	max error	RMSE	max error	RMSE reduction
Coulomb	2.0063	6.1665	0.1697	0.5194	91.54 %
Stribeck	2.1110	5.5305	0.1748	0.4763	91.72 %
Dahl	2.2558	6.1787	0.1652	0.4505	92.68 %
Stefanski et al.	2.1462	6.0054	0.1587	0.4663	92.60 %

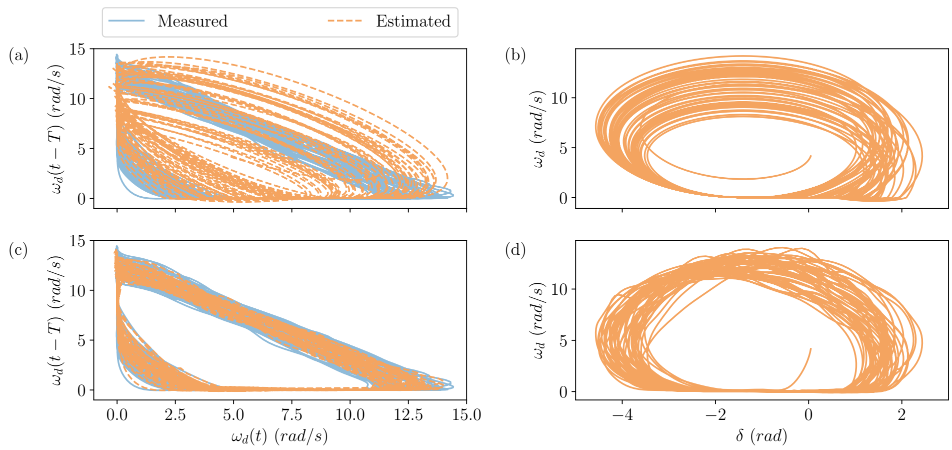

Figure 4.7: Phase-plane portrait of the system dynamics for a reference angular velocity of 5.76 rad/s and an average normal contact force of 50 N: (a) gray-box numerical and experimental reconstructed phase-plane portrait; (b) gray-box numerical phase-plane portrait; (c) ensemble numerical and experimental reconstructed phase-plane portrait; and (d) ensemble numerical phase-plane portrait.

Table 4.3 presents the Root Mean Squared Error (RMSE) and the maximum error for each model type. From these errors, one can verify the improvement achieved by using an ensemble model. Both RMSE and maximum errors decreased compared to the gray-box simulations. At this point, it is interesting to note that if the gray box were sufficiently accurate, the addition of a black-box element would not be capable of improving the predictive performance. The ensemble models constructed with the Dahl and Stefanski et al. friction models presented lower RMSE scores and higher RMSE reduction. However, the Coulomb friction model was selected for further analysis since it performed better in replicating friction mechanisms in the gray-box approach.

Figure 4.7 displays the measured and numerically predicted phase-plane portraits. In Fig. 4.7a and Fig. 4.7c, the numerical and experimental reconstructed phase-plane portraits obtained from the gray-box and ensemble models built with the Coulomb friction model, respectively, are presented. The reconstructed phase-plane portraits are done by plotting $y(t-T)$ against $y(t)$ [53]. The graphs of Fig. 4.7a and Fig. 4.7c were utilized to compare measurements and predictions. Figures 4.7b and 4.7d present the numerical phase-plane portraits formed by plotting the angular disc velocity against the angular difference between motor output and disc.

Comparing Fig. 4.7a and Fig. 4.7c, it is possible to observe that the ensemble model better reproduces the system's dynamical behavior. Moreover, one may visualize that the system follows a bounded trajectory in Fig. 4.7b and Fig. 4.7d, with minor differences in the amplitudes of vibrations for the

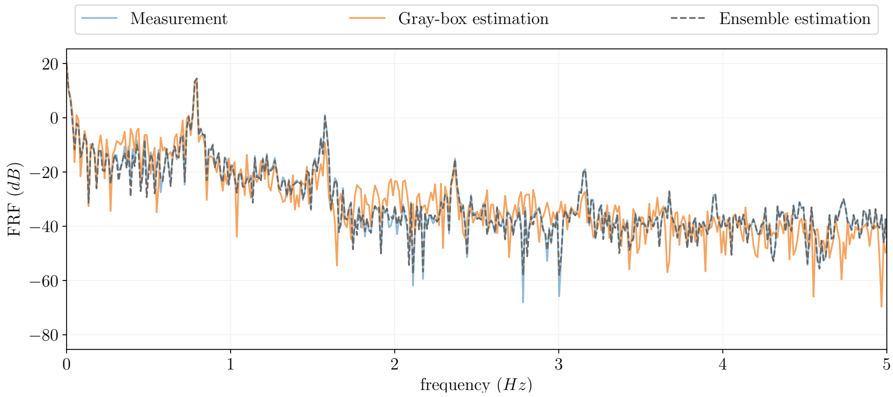

Figure 4.8: Amplitude spectrum of disc angular velocity.

ensemble model.

The numerical simulations reveal the primary vibration frequency at 0.7934 Hz, precisely corresponding to the frequency at which the stick-slip phenomenon occurs. Figure 4.8 displays the amplitude spectrum of the recorded angular velocity, ω_d, as well as the simulated angular velocity, $\hat{\omega}_d$, employing the ensemble model and Coulomb friction. The plot distinctly shows a prominent peak at $f = 0.7934$ Hz, aligning with the anticipated frequency.

In addition, the graph in Figure 4.8 emphasizes that only the ensemble model effectively replicates these specific harmonic frequencies, highlighting its capability to capture the nuanced behavior of the system.

The test rig exhibits different dynamical behaviors depending on its parameters. According to [54, 55, 56] bifurcation diagrams are effective criteria for validating nonlinear system dynamics. To construct bifurcation diagrams, the mean value of the braking device's normal force was varied from 0 to 50 N in steps of 5 N for a reference angular velocity of 5.76 rad/s to observe its influence on the rig dynamics. Figure 4.9 presents both experimental and numerical bifurcation diagrams. In this figure, the maximal and minimal values of angular velocity are plotted when the stick-slip phenomenon is present, and the mean value of the angular velocity when it is not.

Concerning the results, it is possible to make the following remarks:

– For the lower values of the normal force (lower or equal to 20N), the system exhibits oscillations without stick-slip. In the bifurcation diagram, for this region, the points depict the mean value of the angular velocity. In a phase-portrait representation, this would correspond to an orbit around a stable fixed point.

– As the normal force increases so does the amplitude of the torsional oscillations.

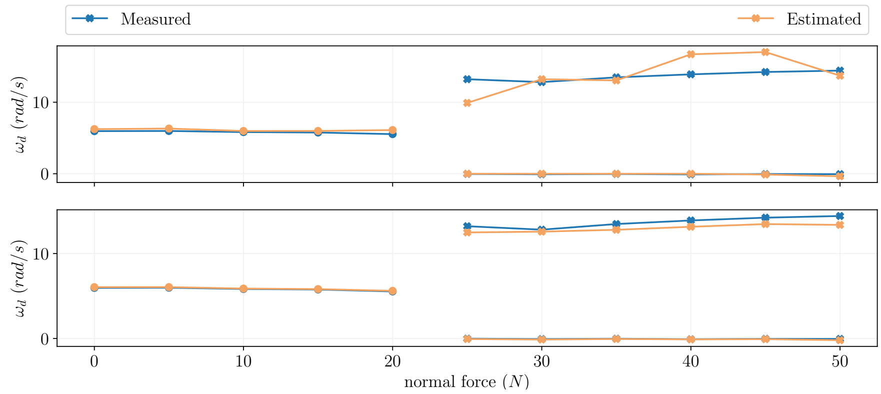

Figure 4.9: Bifurcation diagram with respect to normal contact force for a reference angular velocity of 5.76 rad/s: (top) gray-box numerical and experimental bifurcation diagrams and (bottom) ensemble numerical and experimental bifurcation diagrams.

– After 20N, the stick-slip phenomenon appears due to the nonlinearities in the friction torque at the disc. Further studies should be performed to accurately classify the behavior that the system is exhibiting, although, with the information herein presented and the phase-portrait representation in Fig. 4.7, the authors expect this bifurcation to be Hopf-type. This would mean that the system is following a bounded trajectory that no longer surrounds a stable fixed point.

The aforementioned remarks can be made for both experimental and numerical tests. Comparing the graphs of Fig. 4.9, one may observe that both approaches can determine whether the system is going to present stick-slip oscillations or not. Figure 4.9 indicates that the ensemble model predicts better the amplitude of oscillations. The prediction accuracy of the amplitudes of the vibrations is a relevant aspect since it is directly related to the stick-slip severity, an indicator in the analysis of torsional dynamics in drill strings [57].

4.6 Concluding Remarks

This chapter proposed an ensemble approach for identifying the dynamics of a nonlinear system. The investigated system is a laboratory test rig designed to reproduce the torsional vibration of a drill string in drilling operations. As a first step, the measured responses were used to estimate the unknown rig mechanical parameters and dry contact friction parameters. Next, the error between predictions with the estimated parameters and the measurements was obtained with a black-box technique. Finally, the ensemble model was constructed by adding the black-box component to the physical model.

In the initial step, the cost function was minimized using the CasADi interface with IPOPT. Four distinct friction models of varying complexity were employed to assess their efficacy in capturing the system dynamics. In the subsequent step, parameters for the residuals of the black-box model were estimated. The ensemble model proposed integrates a physics-based approach and an ARX model to encompass aspects of the dynamical response that are not fully captured by the physical model alone. This hybrid approach was embraced to enhance prediction accuracy while retaining interpretability based on physics.

The results of the identification were validated via simulation. The comparison between the friction models showed a difference in the capacity to reproduce stick-slip vibrations. The simulation results demonstrated that the identified system can accurately reproduce the experimental results and that the inclusion of a black-box component effectively attenuates the predictions' inaccuracies by up to 92.68% in terms of RMSE. The bifurcation diagrams prove that both approaches can predict whether the system is going to exhibit stick-slip oscillations or not. The precision improvement inspires additional analysis on ensemble model construction for nonlinear system identification in other challenging applications, such as structural health monitoring [58, 59], and modal analysis [60].

In conclusion, the hybrid approach offers more benefits than uncombined identification techniques, particularly in systems that exhibit vibrations with the stick-slip phenomenon. The analysis proves that, in the ensemble model, different friction models can replicate the bounded trajectory aspect of the friction phenomenon. Further work will be carried out to investigate the existence of a limit cycle. The author believes that the identification results presented in this paper are a significant improvement in the state of the art and may be adequate for analysis and simulation.

5
Data-driven Model for Torsional Oscillations in Slender Structures

This work focuses on the parameter identification of a 2-DOF model to study the torsional dynamics. The system studied is a slender structure subjected to friction. This study calibrates the mathematical model with experimental data. It utilizes an experimental setup composed of a DC motor and two rotating inertias connected by a slender shaft, with friction resulting from braking acting over one of the inertias. The mechanical and friction parameters of the low-dimensional model are inferred using a neural network. Finally, the parameters are compared with those experimentally identified.

5.1
Introduction

Excessive drill string vibration leads to loss of the drilling process effectiveness and premature damage to the equipment: this makes the drilling system behavior a challenge to the process enhancement. The drill string vibrations can either be induced by drill bit-formation or drill string-borehole interactions. Due to the drill string's slenderness, torsional vibration is present in most drilling routines, ultimately reaching the stick-slip phenomenon. Stick-slip is characterized by two phases: one in which the drill bit remains stopped due to the resistive torque, and the other that begins when the stored energy overcomes the resistive torque, and the bit is set in motion.

The stick-slip phenomenon is a complex nonlinear problem since static friction rules the motion during the stick phase, while velocity-dependent kinetic friction rules it during the slip phase ([16]). Despite the complexity of the bit-rock interaction, researchers often treat the relationship between torque and bit velocity as a dry friction function. Surveys on drill string modeling and dynamics can be found in [18, 19]. Most of the mathematical models of slender systems, like drill strings were developed analytically.

This work applies system identification, which comprises a set of techniques for building data-based models ([31]), to calibrate a 2-DOF torsional model. This chapter uses data-driven identification to provide physically interpretable models. The experimental setup utilized is composed of a DC motor and two rotating inertias connected by a slender shaft, with friction resulting from braking acting over one of the inertias. The mechanical and friction parameters of the low-dimensional model are inferred using a neural network. The parameters estimated are compared with those experimentally identified.

5.1.1 Dynamical Model

The experimental system is modeled as a torsional pendulum, considering the resistive torque due to the friction from the braking device as the only torque affecting the system. The resulting equations of motion for the system are:

$$\begin{aligned} J_d\ddot{\theta}_d + c(\dot{\theta}_d - \dot{\theta}_m) + c_d\dot{\theta}_d + k(\theta_d - \theta_m) &= -T_f(\dot{\theta}_d), \\ J_m\ddot{\theta}_m + c(\dot{\theta}_m - \dot{\theta}_d) + c_m\dot{\theta}_m + k(\theta_m - \theta_d) &= \tau_m \end{aligned} \tag{5-1}$$

where the moments of inertia of the disc and the motor are J_d and J_m. The shaft stiffness is denoted by k and the internal damping by c. c_d and c_m are the external dampings. θ, $\dot{\theta}$, and $\ddot{\theta}$ are the angular displacement, angular velocity, and angular acceleration of the inertias, respectively. The torque transmitted to the mechanical subsystem is denoted by τ_m, and the resistive friction torque on disc D2 is denoted by T_f. T_f is given by:

$$T_f = F_f a, \tag{5-2}$$

where a is the distance between the disc center and the disc-pin contact area. For simplicity, $T_C = F_C a$ is considered the resistive torque related to the kinetic Coulomb friction.

5.1.2 Friction Model

The study of the complex characteristics of the bit-rock interaction is indispensable to the drill string dynamics analysis. Despite the complexity of this interaction, studies often treat the torque on the bit as dry friction torque. The friction force is the resistance to the relative motion of two contact surfaces ([13]). [39, 40] include a review of some of the most common models employed in dynamical systems. This study uses the regularized Coulomb friction formulation to obtain the resistive torque T_f that will be used in the dynamical model of the test rig.

The classical Coulomb friction model states that friction opposes the relative motion between contacting surfaces, and its magnitude is proportional to the normal contact force. The following equation defines the unregularized model:

$$F_f = F_C \mathrm{sign}(v), \tag{5-3}$$

where F_f is the friction force, $F_C = \mu_k F_N$ is the magnitude of Coulomb friction, v is, from the perspective of the body, the relative tangential velocity between the contacting surfaces, F_N is the normal force, and μ_k is the kinetic friction coefficient. This model presents a velocity dependence by the sign function that introduces a discontinuity in the system of ODEs. Instead, this study considers a regularized approximation using the hyperbolic tangent with a transition velocity v_t to avoid discontinuities. Therefore, the regularized Coulomb friction is:

$$F_f = F_C \tanh\left(\frac{v}{v_t}\right). \tag{5-4}$$

Because of its simplicity, the regularized Coulomb model is very suitable for System Identification.

5.1.3 Experimental Results

Forces and velocities are measured using a LabView-based Data Acquisition System (DAQ). In Figure 5.1, time histories of motor torque (a), motor inertia angular velocity (b), and disc angular velocity (c) are displayed. The measurements were taken at a nominal angular velocity of 55 RPM and an average normal contact force between the pin and disc of 25 N. This combination results in the system exhibiting stick-slip oscillations, as evident in the graphs of Figure 5.1.

5.2 Methodology

Physical or semi-physical models deal with estimating the physical parameters of a system. To perform the parameter estimation from measurements, this work applies a deep learning approach as proposed in [61]. As input and output data, the torque transmitted from the motor, τ_m, and the angular velocities $\dot{\theta}_d$ and $\dot{\theta}_m$, respectively, are used.

In this study, the motor and disc inertia are assumed to be known, and stiffness, damping, and friction parameters turn into parameters of the physics-informed neural network.

Both motor and disc angular velocities are approximated by deep neural networks. Therefore, the required derivatives are calculated to compute the

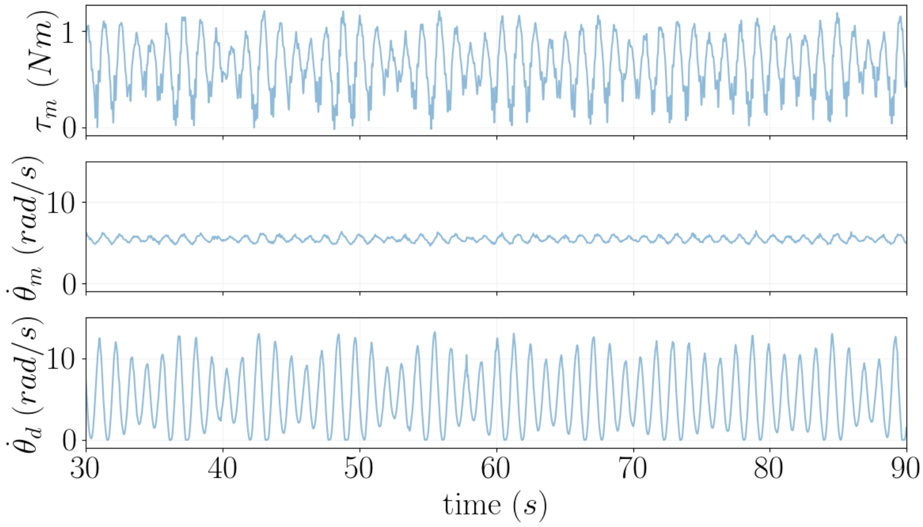

Figure 5.1: Measured time history of (a) motor torque, τ_m; (b) motor inertia angular velocity, $\dot{\theta}_m$; (c) disc angular velocity, $\dot{\theta}_d$.

residual networks applying automatic differentiation. Finally, the physics-informed neural network using (5-1) is obtained. The parameters of the neural networks and the system mechanical and friction parameters are estimated by minimizing the following sum of squared errors cost function:

$$\sum_{i=1}^{N}(y(t^i) - \hat{y}^i)^2 + \sum_{i=1}^{N}(u(t^i) - \hat{u}^i)^2, \tag{5-5}$$

in this cost function, the first summation corresponds to the training data on the output, $y(t)$, and the second summation carries out the dynamic motion equations. In (5-5), y_i and $\hat{y}_i$ are the experimental and predicted data, respectively. The use of deep neural networks is motivated by the advances in solving forward and inverse problems [61].

The applied methodology is exemplified by Fig. 5.2.

5.3
Results and discussion

For system identification, input and output data from the specific 30-90 second timeframe in Fig. 5.1 were utilized. A specialized neural network model, featuring 12 layers with 32 nodes in each, was developed using TensorFlow, a deep learning framework. The training involved optimizing network parame-

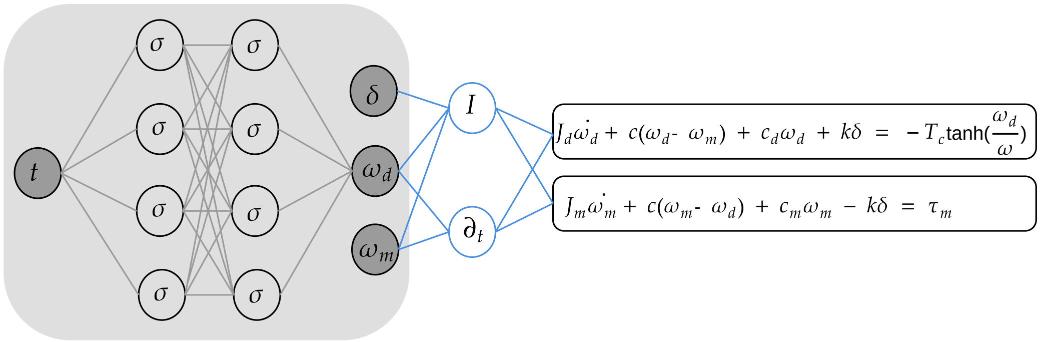

Figure 5.2: Physics-informed neural network.

Table 5.1: Estimated parameters values

	Deep Learning	Experimental Identification
k (Nm/rad)	0.311	0.3482
c (Ns/m)	0	0.0022
c_d (Ns/m)	0	0
c_m (Ns/m)	0	0
T_C (Nm)	0.650	-

ters with the Adam optimizer through four stages of 10,000 epochs each, using a batch size matching the total training samples (6000). The objective was to minimize mean squared error during training, reducing the gap between predicted and actual system responses. The code, written in Python, relied on key libraries like TensorFlow for neural network operations, NumPy for numerical computations, Matplotlib for plotting, and SciPy for effective data handling and manipulation. This effort resulted in a set of estimated parameter values presented in Table 5.1, enabling a comparative analysis with experimentally identified parameters.

Table 5.1 demonstrates a slight variance in the estimated stiffness compared to the experimental value. Notably, the friction parameter was not obtained through experimental tests. However, in deep learning identification, all parameters are acquired simultaneously. The time series reconstruction for disc angular velocity is illustrated in Fig. 5.3.

5.4
Concluding remarks

This work applied physics-informed deep learning to infer the mechanical and friction parameters of the low-dimensional model. The mathematical

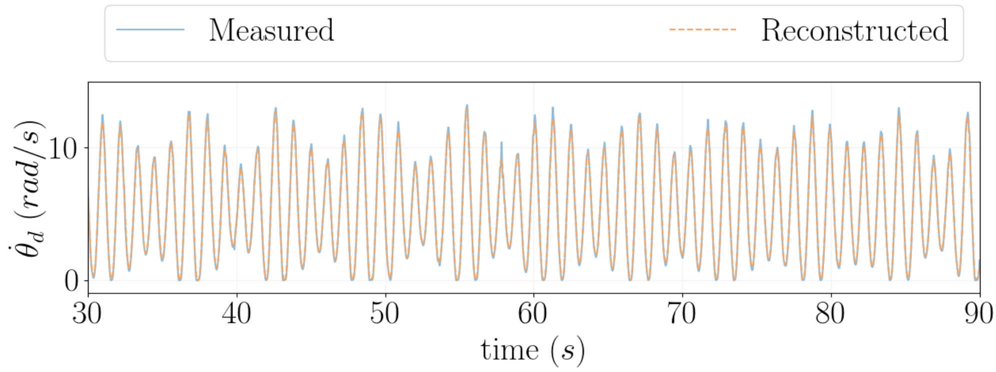

Figure 5.3: Time series reconstruction for disc angular velocity.

model describes a laboratory test rig designed to mimic the torsional dynamics of drilling operations, and it is a slender structure subjected to friction. Because of its simplicity, the regularized Coulomb model was adopted for system identification.

Besides the excellent reconstruction of the time series for angular velocity, the methodology employed is capable of identifying the values for stiffness, damping, and friction parameters. The obtained values were compared with those experimentally identified.

6
Experimental studies of coupled axial and torsional oscillations of slender structures

6.1
Introduction

Drill strings are critical components in drilling operations, and understanding the coupled oscillations, specifically axial and torsional oscillations, is essential for optimizing drilling performance and ensuring operational safety. Over the years, numerous experimental studies have been conducted to investigate the dynamics of coupled oscillations in drill strings [9].

Drill strings can be divided into three main sections from a structural perspective. The first section is comprised of the drill pipes, which are a series of tubes responsible for transmitting the power generated by the motor at the top of the well to the lower components. Typically, the total length of the drill pipes varies between 1 to 10 kilometers. The second component is the bottom hole assembly (BHA), which consists of thick-walled tubes designed to provide the necessary weight-on-bit (WOB) during the drilling process. Additionally, the BHA often includes devices used for measuring and controlling the direction of the bit. The third element is the bit itself, responsible for cutting the formation [5].

During the drilling process, self-excited vibrations can manifest in three forms: axial, lateral, and torsional vibrations. These vibrations can result in detrimental effects such as bit bouncing, whirling, and torsional stick-slip, which can lead to premature component failures. This study focuses on the coupling between torsional and axial vibrations, acknowledging the significance of understanding their interaction.

The experimental setup utilized in this chapter is well-established in the literature, and numerous previous works have extensively investigated its different facets. In [62], the authors delve into the analysis of drill-string dynamics by combining theoretical modeling with experimental investigations. Their study explores the effects of drilling parameters on the stability and dynamics of drill strings, shedding light on the complex behavior observed during experiments. The same authors focus on understanding forward and backward whirls in drill strings in [63], where they experimentally investigate the occurrence and characteristics of whirl vibrations, examining the influence of drill string parameters and operating conditions. Moreover, in the pursuit of unraveling the complexity of drill string vibrations, [64] takes an experimental and modeling approach. Laboratory experiments are conducted to characterize the nonlinear dynamics of drill strings and validate the developed mathematical models. These findings contribute to a deeper understanding of the complex dynamics involved in coupled oscillations.

Several additional experimental studies have been conducted to investigate drill string vibrations. The authors of [65] utilized a slender rotating structure and measured vibrations using sensors to identify the underlying nonlinear dynamics caused by friction-induced vibrations. [66] explores the effects of different drilling parameters and operating conditions on drill string vibrations, providing valuable insights into their behavior under various circumstances. [67] focuses on stick-slip vibrations in drilling with drag bits, conducting experimental studies to examine the characteristics and mechanisms of this detrimental phenomenon. The authors of [68] investigated the construction of an autonomous laboratory-scale drilling rig, which served as a controlled environment for experimental studies on drill string vibrations, allowing for in-depth analysis and understanding of coupled oscillations. Additionally, [69] concentrates on the vibrational behaviors of horizontal drill strings, employing experimental investigations to analyze the characteristics and factors influencing vibrations in horizontal drilling operations.

However, it is important to note that not all of the experimental studies mentioned in the literature specifically address the coupling between axial and torsional oscillations. Among those that do, certain noteworthy findings can be highlighted. Some experimental rigs employ shakers at the extremity to provide constant axial displacement amplitude excitations [66]. Conversely, in the case of horizontal rigs, such as in the study conducted by Lin et al. [69], axial vibrations are not as significant due to the radial direction of gravity. Therefore, conducting a meticulous experimental investigation of the coupling mechanism of vibrations utilizing a vertical rig that employs actual drill bits and rock samples would be of great value.

This chapter is the result of a cooperation between Prof. Hans I. Weber from PUC-Rio University and Prof. Marian Wiercigroch from the University of Aberdeen and focuses on the experimental investigations conducted using a specially developed drilling rig at the Centre for Applied Dynamics Research, University of Aberdeen. The rig's configuration was customized specifically for the purposes of this study. The adaptation of the setup was a collaborative effort between the author and the CADR team. The primary objective is to replicate and study fundamental modes of vibrations observed during drilling, specifically torsional and axial vibrations. The chapter begins by introducing the key components of the drilling rig. These components include the drilling machine, flexible shafts that approximate the drill string, drill bits, and the availability of rock samples for testing. Subsequently, the experiments are described, highlighting the specific measurements of interest and the data acquisition system employed to collect the experimental data. The next step involves identifying the essential system parameters, such as the stiffness and damping characteristics of the flexible shafts, which play a crucial role in the dynamics of the drilling rig. Lastly, the chapter presents examples of different types of system responses observed during the experiments. These examples encompass various scenarios of torsional and coupled oscillations, illustrating the range of dynamic behaviors exhibited by the drilling rig.

6.2 Aberdeen drill string dynamics experimental rig

This section describes the experimental setup developed in the Centre for Applied Dynamic Research (CADR) laboratory at the University of Aberdeen, which was used to acquire the experimental data presented in this chapter. The experimental bench of CADR is widely known in the literature, with several works exploring its various aspects. It is explained here, but more details are explored in the contributions of its developers [64, 62]. The intent of the experimental rig is to provide a comprehensive test bed for the investigation of different types of undesired vibrations associated with the operation of an oil drilling column.

This work aims to investigate, in a practical manner, the coupling between axial and torsional oscillations, and the influence of certain parameters on the phenomena of interest For this purpose, the experimental apparatus was modified. Figure 6.1 shows a picture and the schematics of the new configuration of the rig, indicating the main components of the setup. The author collaborated with the CADR team to modify and adapt the setup.

The experimental system is composed of a drilling machine, two flexible shafts, a steel cylinder, BHA, a drill bit, and a rock sample. The drilling machine is located at the top of the column and provides the angular and axial displacement to perform drilling. Steel cables are used to transfer the motion from the motor to the system as they have high torsional rigidity and low flexural rigidity. As Fig. 6.1 shows, one of the cables is connected to the motor at the top and at the bottom to the steel cylinder placed at the hub of

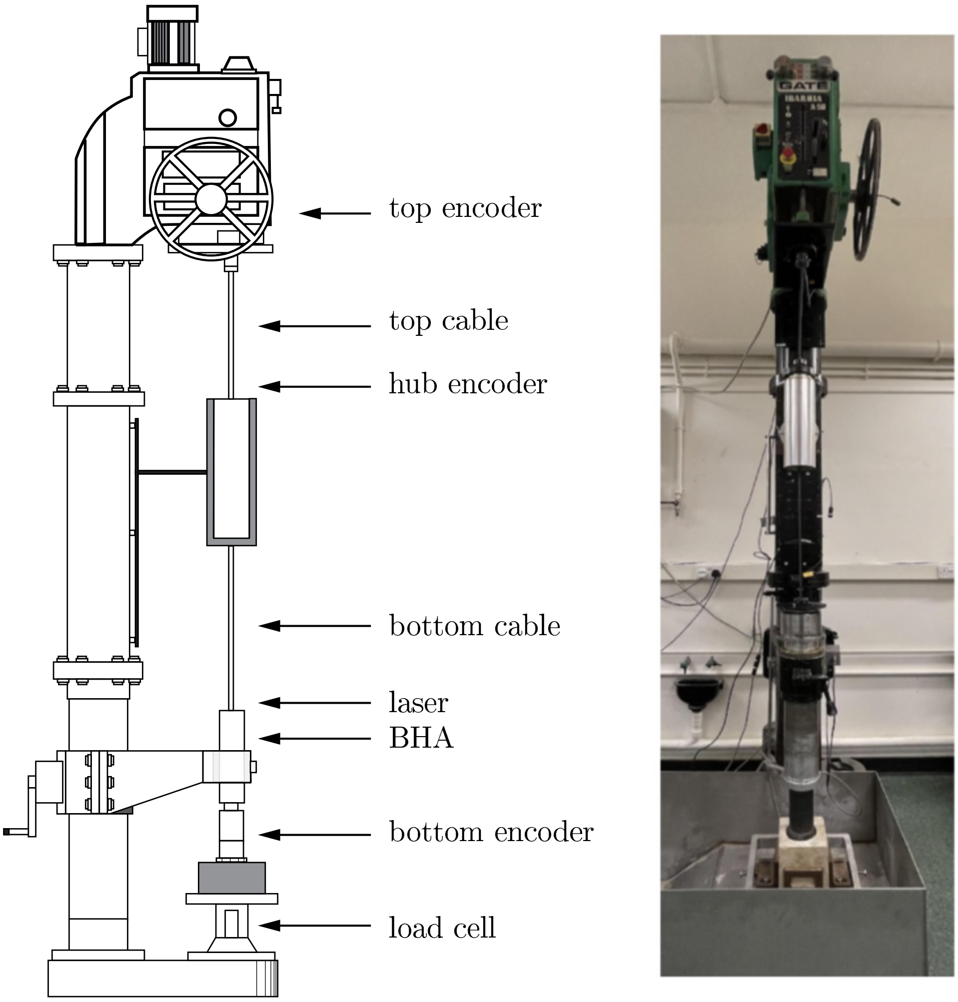

Figure 6.1: Picture of the test rig's latest configuration, accompanied by detailed schematics.

the rig, and the other cable connects the cylinder to the BHA, which is another steel cylinder, where the drill bit is fastened. Moreover, the experimental setup may be used with several different industrial drill bits as well as different rock samples with varying compositions, allowing for the investigation of numerous scenarios. For the experimental tests realized for this work, a PDC bit and a sandstone sample were used.

For data acquisition, the system is equipped with three identical encoders of quadrature type to measure angular displacement in different positions; a Kistler 9272 four-component dynamometer, which is placed beneath the rock sample to measure the WOB and TOB; a laser, to measure the axial displacement of the drill bit (Fig. 6.2); and two Eddy current probes, positioned 90° apart on the sides of the bearing in the BHA in order to capture its

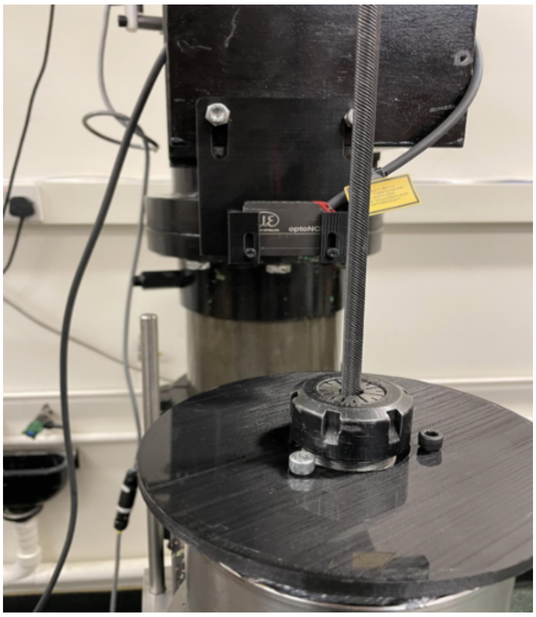

Figure 6.2: A photograph showcasing the laser positioned above the BHA.

lateral displacements. It's important to note that this study did not include measurements for Weight on Hub (WOH) and Torque on Hub (TOH), and implementing further modifications is necessary to enable the measurement of these signals. The sensors communicate with an interface developed in LabView through a National Instruments acquisition board and are installed as shown in Fig. 6.1

6.3 Experiments

This section delves into the examination and analysis of several experimental studies carried out using the CADR laboratory's experimental setup. As previously mentioned, the CADR experimental setup is a valuable resource for conducting experimental investigations, as it replicates diverse types of undesirable drill string vibrations.

The experimental investigations conducted in this study involved conducting a sweep of the top speed of the drill string, ranging from 0 to 54 rpm. Data regarding angular positions, and the axial position of the bottom BHA, WOB, and TOB were recorded using LabView. The recorded angular displacements were then used to calculate angular velocities through differentiation performed in MATLAB. Throughout these experiments, different torsional and axial vibrations were observed depending on the applied angular velocity.

6.3.1 Parameters identification

Accurate estimation of the physical parameters of the experimental apparatus is crucial for achieving good agreement between experimental observations and numerical predictions. This subsection provides a detailed explanation of the mechanical parameter identification process. Figure 6.3 presents schematics of the test rig indicating some geometrical aspects.

The moments of inertia were determined by treating the steel cylinders as rigid bodies and considering their physical properties. Table 1 displays the measured parameters along with the calculated moments of inertia.

Table 6.1: Masses and moment of inertia

	m $[kg]$	J $[kg.m^2]$ (10^{-3})
hub	4.532	5.382
BHA and bit	18.641	18.9

As explained in section 6.2, flexible shafts are used to imitate the mechanical properties of slender structures like drill strings. Due to the length of a drill string, the transversal stiffness of the structure, when compared to the axial one, is negligible. The kind of shafts used are utilized to transmit power in rotating machines as they have high torque capacity transmission and high flexibility. In this research, two flexible shafts with diameters of 8 mm were used, one of the cables connects the motor at the top to the steel cylinder placed at the hub of the rig, and the other cable connects the cylinder to the BHA, as depicted in Figure 6.1.

To find out the torsional stiffness and viscous damping of the shafts, an initial angular displacement was applied, separately, to the inertia and measured the decaying free torsional oscillations. Figure 6.4 plots both shafts' responses. It is worth mentioning that the motor was mechanically locked to get the hub response, likewise, to get the response of the BHA, the rotation of the hub was restricted. The free responses are then used for estimating the damped and natural frequencies, and the damping coefficients.

The damping ratio, ξ, was computed using the logarithmic decrement described in (6-1) and (6-2) [70].

$$\upsilon = \ln\left(\frac{\delta_i}{\delta_{i+1}}\right), \tag{6-1}$$

$$\xi = \frac{\upsilon}{\sqrt{(2\pi)^2 + \upsilon^2}}, \tag{6-2}$$

where δ_i and δ_{i+1} are the ith and $ith+1$ amplitude peaks, respectively.

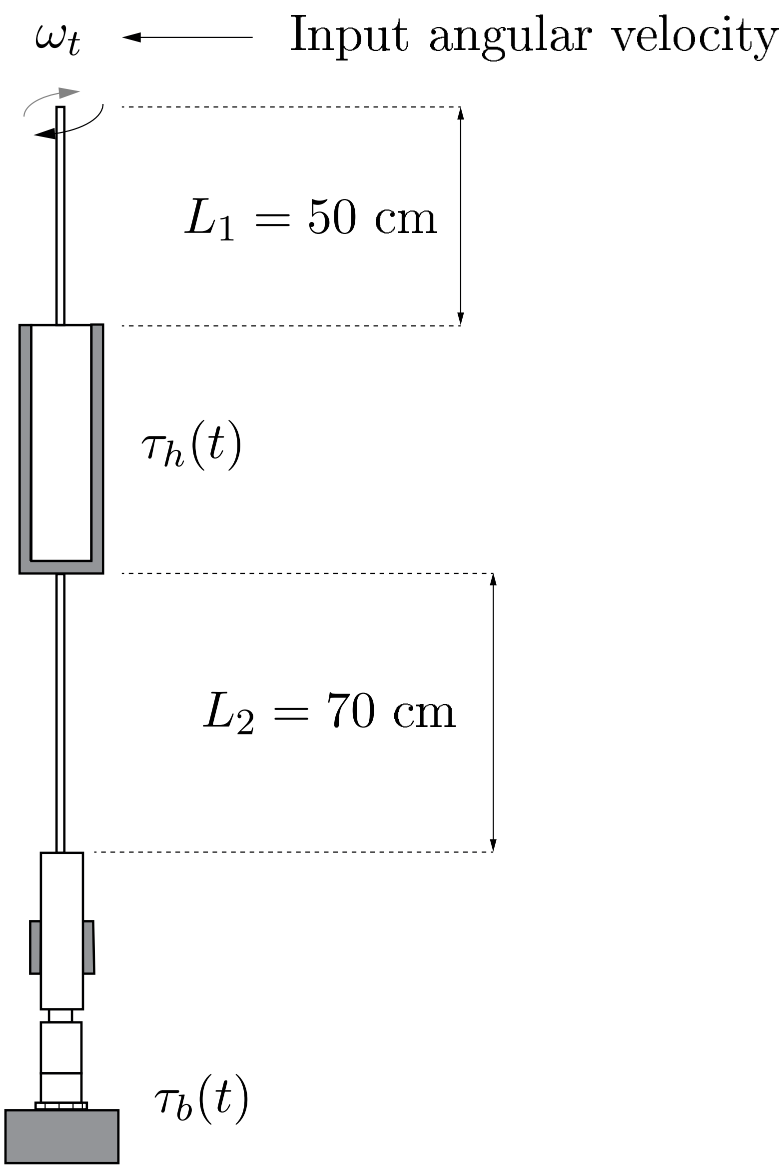

Figure 6.3: Depiction of the utilized test rig.

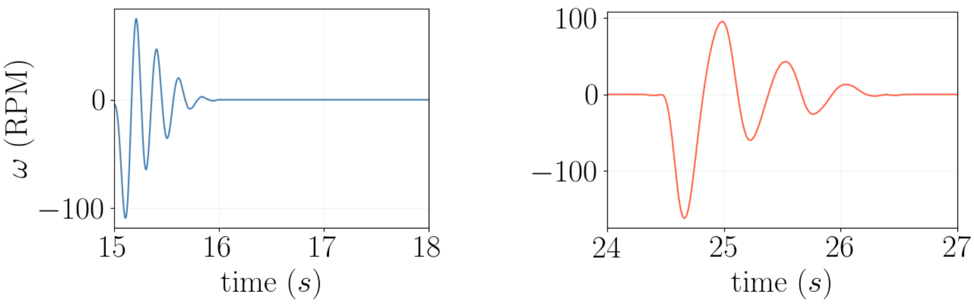

Figure 6.4: Free torsional oscillations: assessing stiffness and damping characteristics of the flexible shaft through initial torsional deformation. (a) top part and (b) bottom part.

The natural frequencies, stiffness, and damping coefficients were calculated using (6-3), (6-4), and (6-5), respectively [70].

$$\omega_n = \frac{\omega_d}{\sqrt{1-\xi^2}}, \tag{6-3}$$

$$k = \frac{\omega_n^2}{J}, \tag{6-4}$$

$$d = \xi(2J\omega_n). \tag{6-5}$$

Table 6.2 contains the natural frequencies, the stiffness, and damping coefficients estimations.

Table 6.2: Natural frequency, stiffness, and damping calculations.

	ω_n $[rad/s]$	k $[Nm/rad]$	d $[Ns/m]$
top cable	31.1	5.22	4.41
bottom cable	11.52	2.51	6.31

6.3.2 Experimental study of different torsional motions

One of the objectives of this study is to investigate the stick-slip phenomenon, and for this purpose, 8mm flexible shafts were adopted. During the conducted experiments, different torsional vibrations at various applied angular velocities were observed for two different configurations. In the first configuration, the only resistive torque present in the system was the dry friction between the cylinder at the hub and its support, with no contact between the bit and the rock sample. In the second configuration, both contacts (at the hub and the bit) were present. The decision to analyze only one point of contact

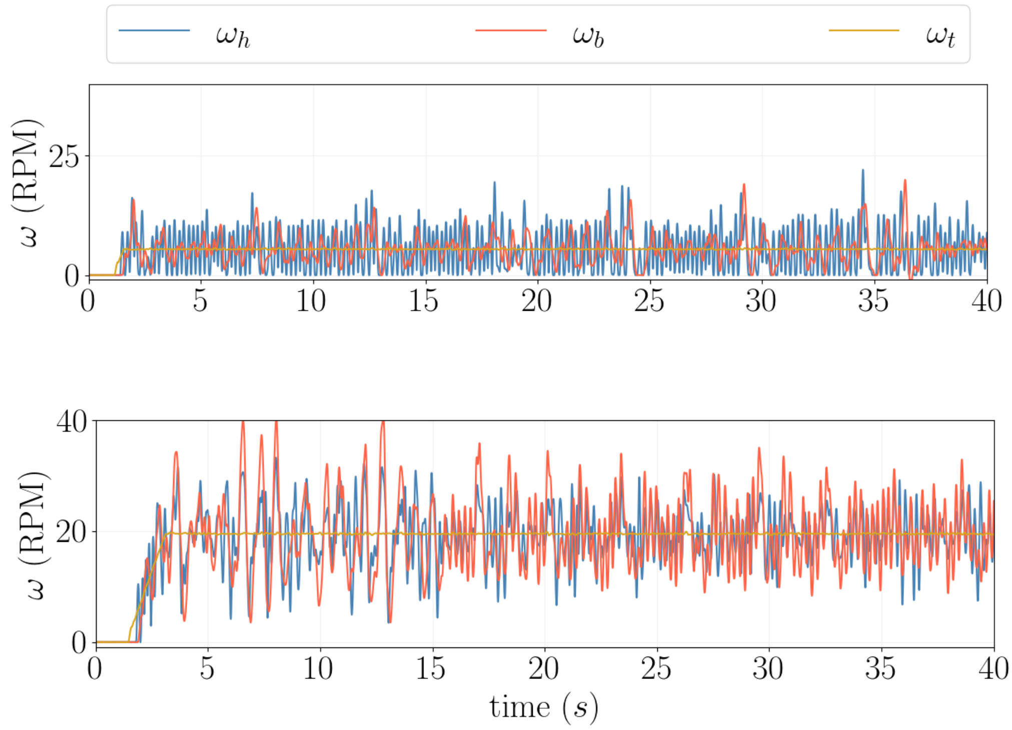

Figure 6.5: Example of different types of torsional oscillations: (a) $\omega_t = 5$ RPM and (b) ω_t 20 RPM.

was motivated by two reasons: firstly, to model the dry friction torque at the hub, and secondly, to understand its influence on the dynamics of the system.

The influence of the motor angular speed on the two configurations was examined. Regarding the first configuration, Fig. 6.5 illustrates the two distinct behaviors observed during the tests, each recorded for a duration of 40 seconds. To provide a closer look at the results presented in Figure 6.5, Figure 6.6 zooms in on a 10-second window. Figures 6.5 and 6.6 depict the angular velocity applied at the top by the motor and captured by the upper encoder (ω_t), the angular velocity at the hub (ω_h), and the angular velocity of the bit recorded by the lower encoder (ω_b).

In Figure 6.5, the motor's angular velocity (ω_t) is approximately 5 rpm in the top results and around 20 rpm in the bottom results. The system exhibits distinct behavior for these different velocities. In the case of the lower velocity (Figure 6.5a), the stick-slip phenomenon is observed, evident from the hub and drill's angular velocity both assuming zero values and remaining in that state for a short period. On the other hand, for the higher velocity, significant oscillations of the bit speed are observed around the angular velocity set by the motor, but stick-slip is not observed.

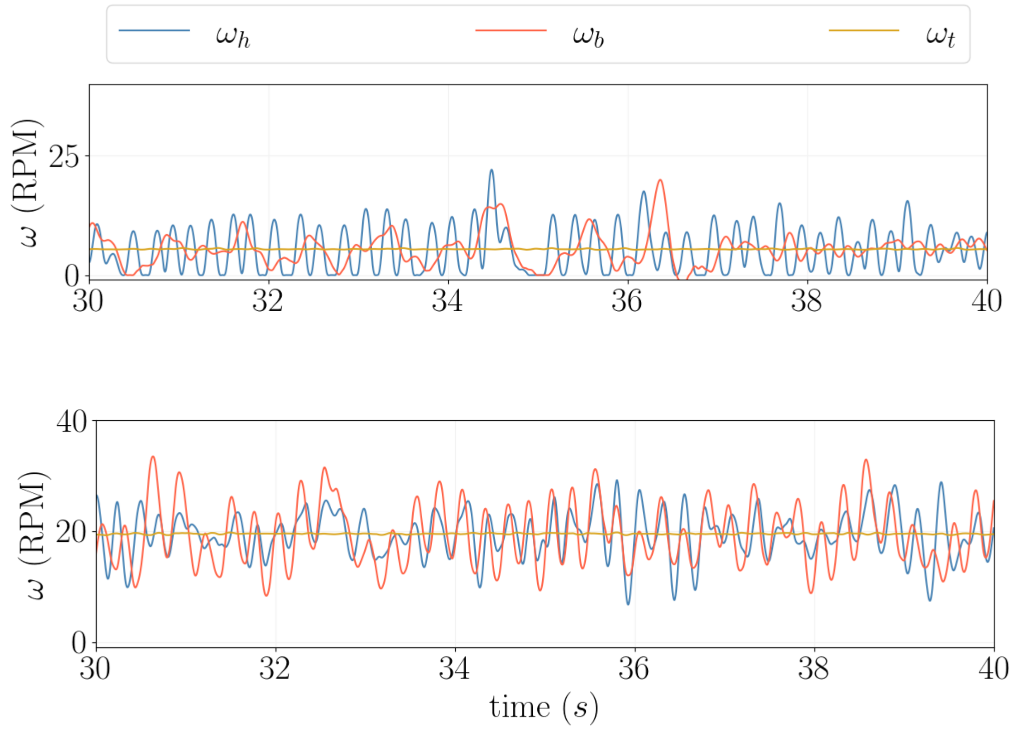

Figure 6.6: Zoomed-in example of different types of torsional oscillations: (a) $\omega_t = 5$ RPM and (b) ω_t 20 RPM.

A similar analysis was conducted for the case where both contact points, hub-wall, and bit-rock, are considered. Figure 6.7 depicts the different behaviors observed in the tests, each recorded for 120 seconds. Additionally, Figure 6.8 provides a closer view of a 10-second window of the data.

Figure 6.7 presents the motor's angular velocity (ω_t) at approximately 13.5, 27, 40.5, and 54 rpm in graphs a, b, c, and d, respectively. The results highlight the impact of the investigated parameter on the system's behavior. The angular velocity applied to the rig has a significant influence on the system's dynamics, leading to diverse torsional vibrations and, in certain instances, causing stick-slip phenomena. The graphs in Fig. 6.8 provide a closer view of the system's dynamics, revealing two distinct behaviors. The results displayed in Figure 6.8a and 6.8b clearly exhibit the occurrence of the stick-slip phenomenon. In Figure 6.8a, it is evident that when the drill experiences the slip effect, its rotational speed reaches values close to 45 rpm, which is more than three times the speed set by the motor. To prevent stick-slip under the given WOB condition, the motor's rotation speed was adjusted. The resulting behavior, as depicted in Figure 6.8d, shows a completely different pattern characterized by a circular phase portrait, where stick-slip is absent.

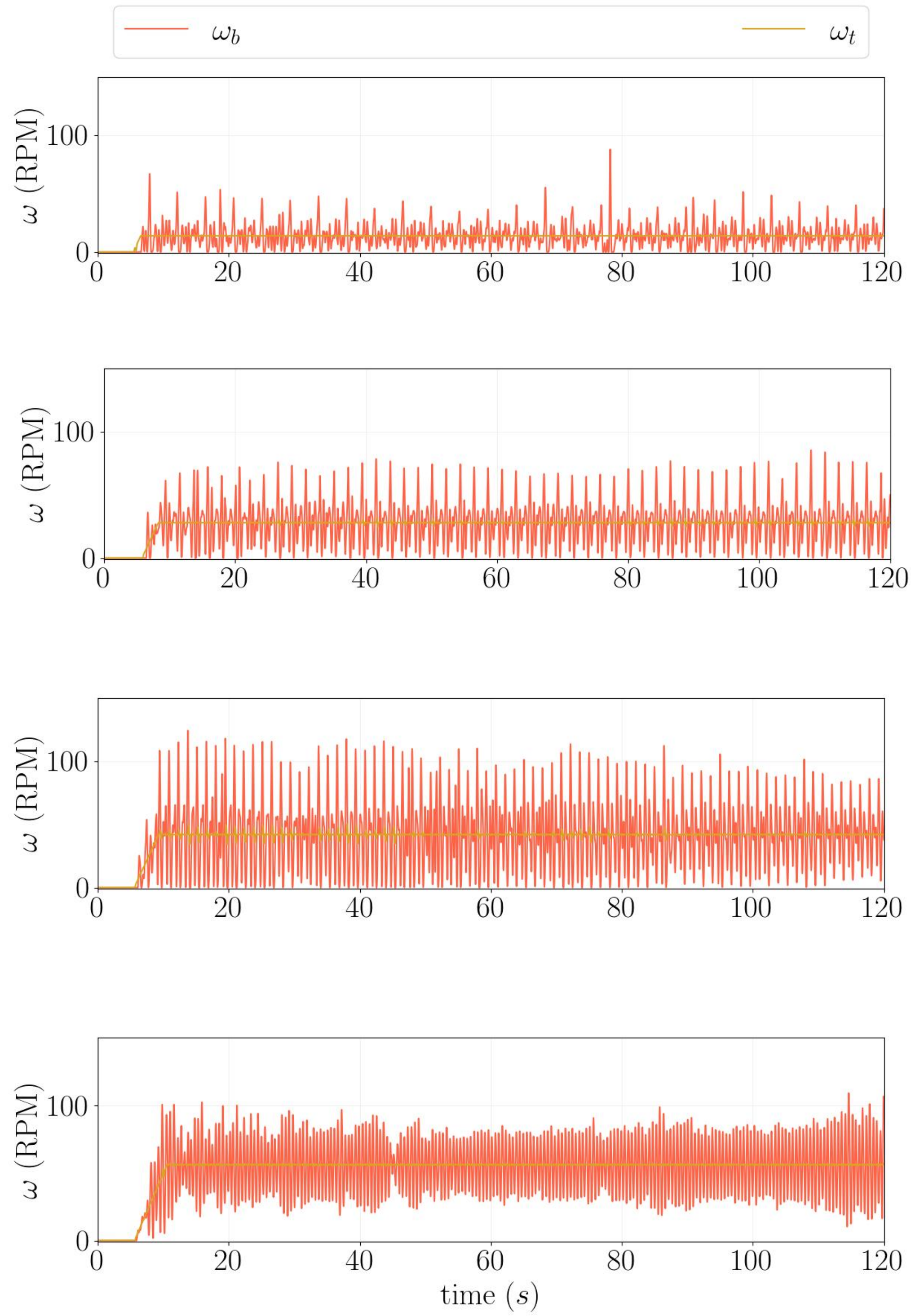

Figure 6.7: Example of different types of torsional oscillations: (a) $\omega_t = 13.5$ RPM, (b) ω_t 27 RPM, (c) $\omega_t = 40.5$ RPM, and (d) $\omega_t = 54$ RPM.

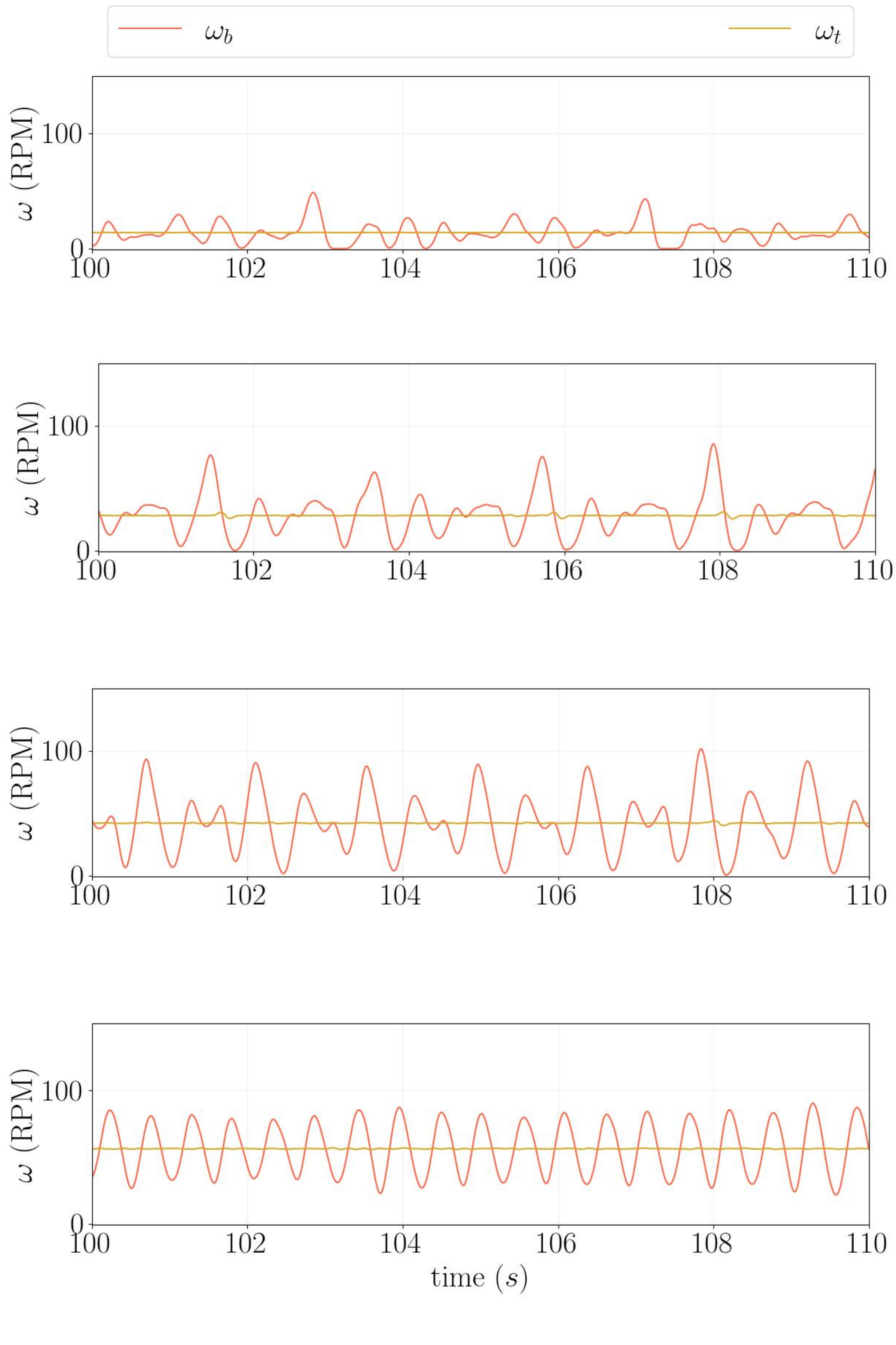

Figure 6.8: Zoomed-in example of different types of torsional oscillations: (a) $\omega_t = 13.5$ RPM, (b) ω_t 27 RPM, (c) $\omega_t = 40.5$ RPM, and (d) $\omega_t = 54$ RPM.

The experimental analysis revealed the presence of the stick-slip phenomenon under various WOB conditions and top angular velocities. However, it was observed that stick-slip tends to diminish with an increase in the top angular velocity, as illustrated in Figure 6.7.

6.3.3 Experimental study of coupled oscillations

In this study, the focus lies on experimentally investigating the coupling between torsional and axial vibrations in drill strings. The coupling between these vibration modes is a complex phenomenon influenced by various factors, including changes in axial load and torque, friction and contact forces, and drill string properties. Understanding this coupling behavior is crucial for optimizing drilling operations and mitigating vibrations. Unlike previous works utilizing pre-buckled configurations, this study introduces a new configuration with a cylinder at the hub to examine the coupling between vibration modes. The nonlinear interactions between the hub and wall, as well as the bit and rock samples, result in helical buckling and axial displacement without relying on pre-existing buckling. The findings, illustrated in Figure 6.9 and a closer view in Figure 6.10, provide valuable insights into the coupled vibrations observed in the system.

The experimental results captured for a duration of 60 seconds with an applied angular velocity of approximately 16.2 rpm are presented in Fig. 6.9. The observed behavior of the system is notably distinct from previous observations. Figure 6.9(a) illustrates the angular velocities (ω) of the top, hub, and bit, while Fig. 6.9(b) displays the axial displacement (x) of the bit. Additionally, Fig. 6.9(c) and 6.9(d) represent the WOB and TOB, respectively. To provide a closer view of the data, a 10-second window is presented in Figure 6.10, plotting the same results.

It is important to note that for the conducted test, both cables were subjected to tension. From the observations in Fig. 6.9, it can be concluded that the system exhibits stick-slip phenomena. This means that resistive torques cause the bit to come to a halt, while the top drive continues rotating until the stored energy surpasses the resistive torques, initiating the motion of the bit. Consequently, the rotational speed of the bit transitions from rest to approximately 50 rpm, which is more than three times the imposed velocity. As a result and a consequence of these torsional oscillations, axial oscillations are observed. The axial oscillation is measured from the laser to the bit, as depicted in Fig. 6.2, where a higher value of x corresponds to a lower position of the bit.

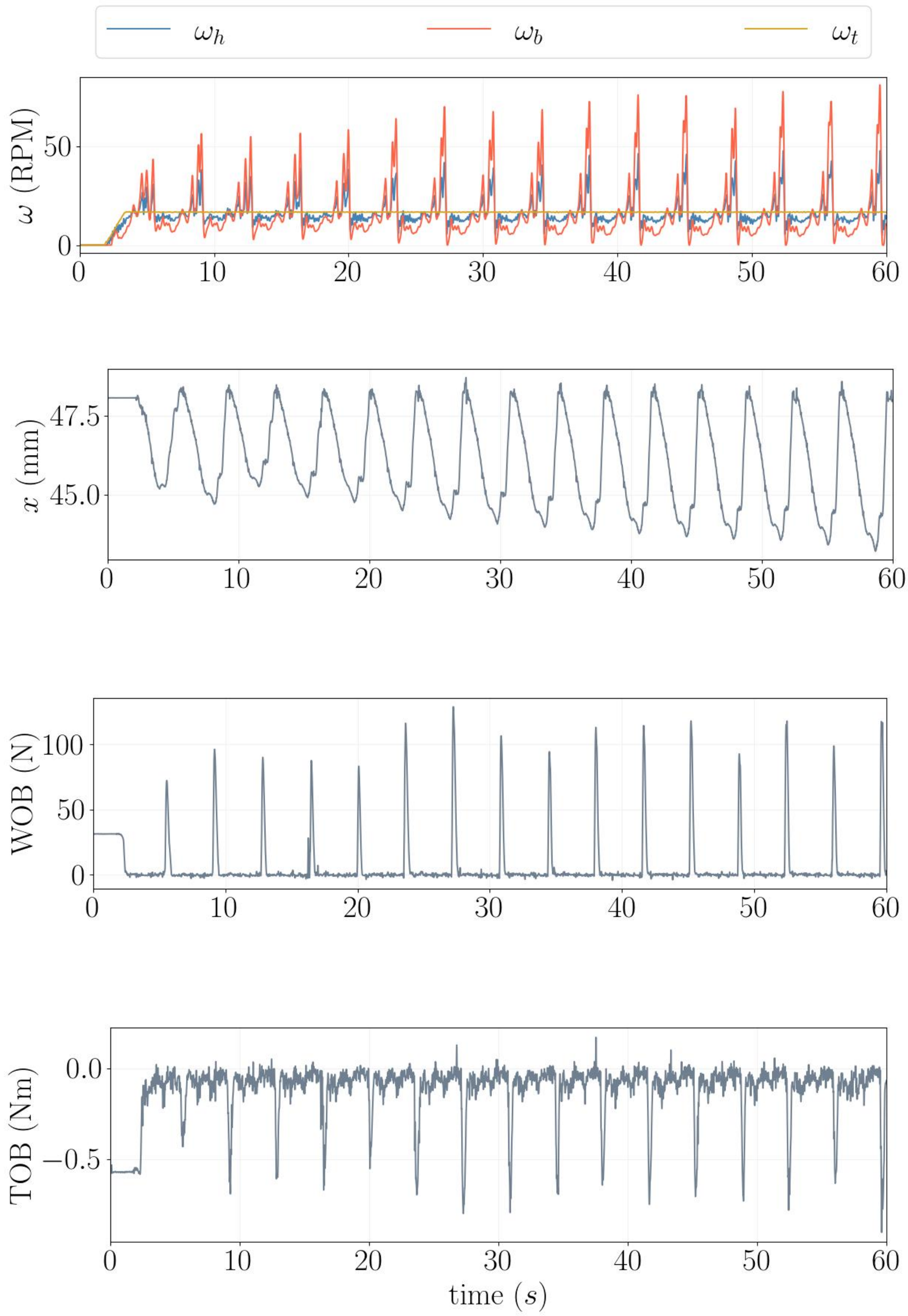

Figure 6.9: Analysis of system response for the selected set of parameters: time histories of (a) angular velocities for top, hub, and bit (marked in yellow, blue, and red, respectively); (b) bit axial displacement; (c) WOB; and (d) TOB.

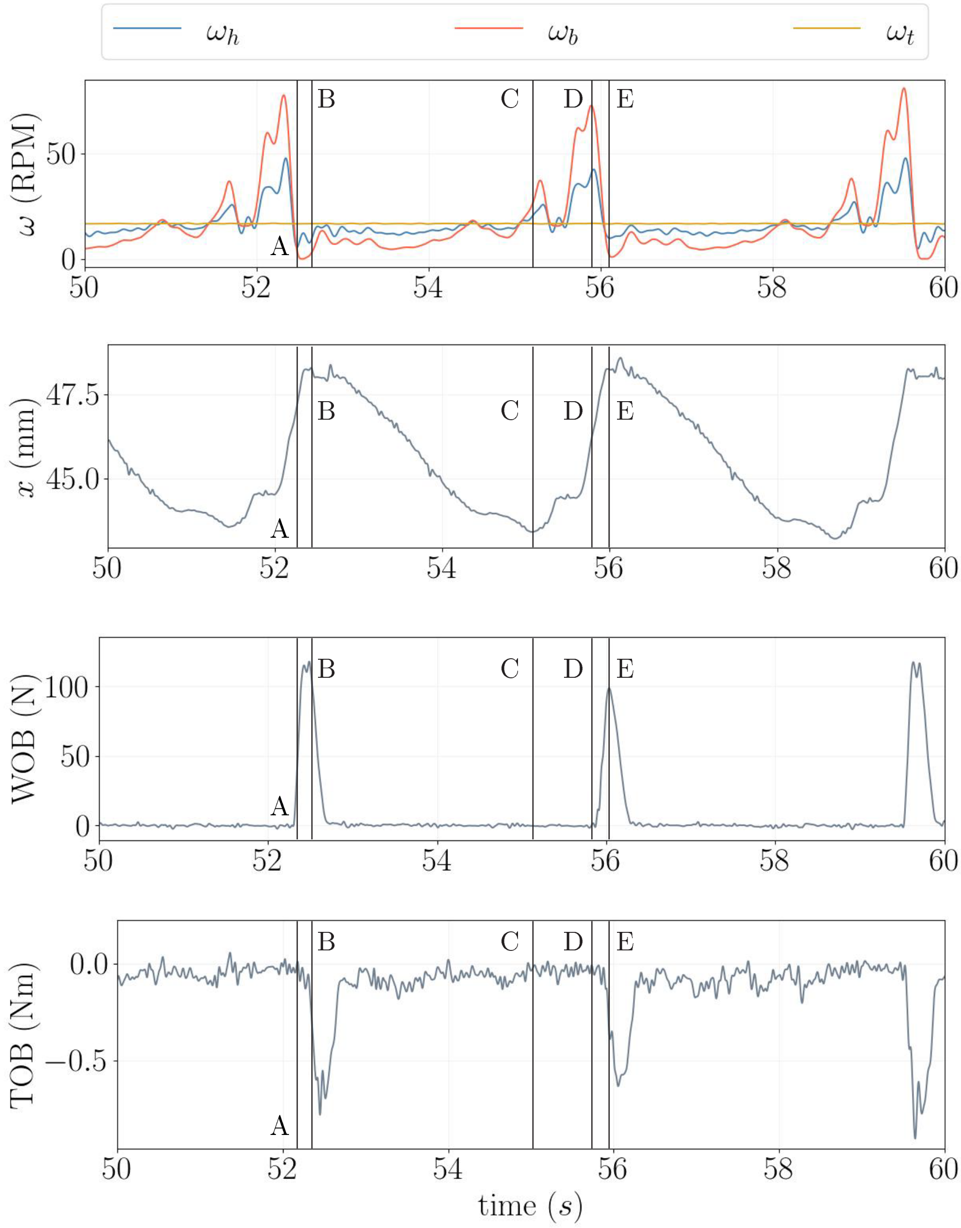

Figure 6.10: Zoomed-in time histories of (a) angular velocities for top, hub, and bit (marked in yellow, blue, and red, respectively); (b) bit axial displacement; (c) WOB; and (d) TOB.

The observed behavior can be attributed to the dynamics of the new configuration, which differs from previous studies. Previous studies in this test rig solely considered the bit-rock interaction, whereas, in this study, the additional hub-wall contact introduces additional resistive torque to the system. This hub-wall contact simulates the contacts between the drill string and the wellbore wall encountered in directional drilling. As a result of this additional resistive torque, more energy is required to overcome the resistance and initiate the movement of the bit.

The sensors integrated into the experimental setup allow for a more detailed investigation of the coupling between the mechanisms. Figure 6.10 is employed to analyze the TOB and WOB in conjunction with the drill's rotational speed and axial position. To facilitate the analysis, five points of interest, labeled A, B, C, D, and E, are identified.

Point A represents the occurrence of bit sticking, indicating the region between A and B as the stick region. During this phase, the motor's rotation speed, depicted in yellow, continues uninterrupted. Consequently, the flexible shaft absorbs and stores the energy supplied by the motor, leading to an increase in TOB, as observed. The stuck bit results in energy accumulation within the flexible shaft, which is subsequently transferred from torsion to other directions, causing the shaft to adopt a helical configuration. This helical buckling effect causes the entire system to move upwards. Consequently, the momentarily loosened bit leads to a rapid decrease in torque, approaching values close to zero, which is also reflected in the WOB. Only when the accumulated energy surpasses the resistive torque of the drill, does it exit the inert state and resume rotation, entering the slip region.

Once the accumulated energy surpasses the resistive torque, it is released in kinetic form, denoted by point B. Within the region from B to C, the bit rotates at low angular velocities, while still moving upward. Notably, both the WOB and TOB remain at zero during this phase.

Within the region from C to D, notable observations include the bit rotating at higher velocities while moving downward, resulting in an increase in both WOB and TOB. At point D, the bit reaches a rotational speed of approximately 80 rpm, which is a direct consequence of the accumulated energy stored in the flexible shaft during the period of drill obstruction. The phenomenon known as "bit-bounce" becomes apparent between points B and D.

In the final phase, from point D to point E, the resistive torque caused by friction begins to act in the opposite direction of the drill's rotation. As a result, the energy released during the slip region is dissipated. This dissipation leads to a gradual reduction in the rotation speed. As the system approaches the stick region once more, the helical configuration of the flexible shaft is undone, and the bit returns to its initial position. With the drill's rotation being obstructed again, the cycle restarts, initiating a new sequence of stick-slip and bit-bounce behavior.

Hence, the presented and discussed results hold significant value as they facilitate an experimental investigation, discussion, and comprehension of the phenomena documented in the literature and previously studied numerically in the next section.

6.4 Conclusions

In conclusion, this chapter has presented the experimental investigations conducted at the University of Aberdeen, aimed at exploring the coupling between torsional and axial oscillations in slender structures. The experimental setup was carefully modified and adapted to facilitate the study of this coupling phenomenon, enabling us to gain a deeper understanding of the dynamic behavior of the system.

Utilizing sensors to monitor and analyze the system's behavior, with a specific focus on the influence of imposed angular velocity parameters, it is possible to extract valuable insights from the experimental data. The observations made during these investigations shed light on the intricate interactions between torsional and axial vibrations, providing crucial information for our overall research.

The combination of experimental tests and data analysis has proven to be instrumental in comprehending the coupling mechanism within the drill-string systems. These insights will significantly contribute to the development of accurate mathematical models and further our understanding of the torsional vibrations and stick-slip phenomenon in slender structures.

7
Conclusions and Recomendations

7.1
Conclusions

This research gave emphasis to studying torsional vibrations and analyzing the stick-slip phenomenon. Self-excited vibrations are a common occurrence during the drilling process, with axial, lateral, and torsional vibrations being the main types. These vibrations can have negative consequences such as bit bouncing, whirling motion, and torsional stick-slip, which can result in early wear and tear of drilling components.

The main objective of this thesis (as stated in Section 1.2) is to explore torsional and axial oscillations using two laboratory-scale experimental test rigs. The focus of the research is to gain a deeper understanding of these types of vibrations and their behavior in controlled experimental settings. By conducting experiments on these rigs, the thesis aims to provide valuable insights into the dynamics and characteristics of torsional and axial oscillations in drilling systems.

The thesis makes significant contributions in several areas related to the investigation of torsional and axial oscillations. Firstly, it focuses on the experimental analysis of lab-scale drill-string systems, providing valuable insights into the dynamics and behavior of such systems. Secondly, it involves the development of mathematical models specifically designed to capture torsional vibrations in slender systems, improving our understanding of their characteristics. Thirdly, the thesis proposes and explores system identification strategies for nonlinear systems, enhancing our ability to accurately estimate and predict system parameters. Finally, the proposed identification methods are experimentally validated, demonstrating their effectiveness in practical applications. The contributions of this thesis can be summarized as follows:

– As a first contribution, an analysis of the torsional behavior of an experimental rig developed at Pontifícia Universidade Católica do Rio de Janeiro was conducted. The rig was designed to replicate the torsional dynamics observed in real drilling systems. To investigate the system's behavior, a mathematical model representing the rig as an actuated torsional pendulum was employed. Specifically, it focuses on examining the influence of the control parameters, namely the reference angular velocity and the normal contact force, on the system's response. This analysis aimed to identify the conditions under which the stick-slip phenomenon is more likely to occur. Based on the results presented in this study, it is possible to conclude that the stick-slip phenomenon tends to manifest at low values of the reference velocity and high values of the normal contact force.

– This thesis proposed an ensemble approach for identifying the dynamics of a nonlinear system, specifically focusing on a laboratory test rig designed to replicate torsional vibration in drill string systems. The approach involved estimating mechanical and friction parameters using measured responses and minimizing a cost function. The work compared different friction models and incorporated a black-box component to enhance the accuracy of predictions. Simulation results validated the identification, showing that the ensemble model effectively reduced predictions' inaccuracies and accurately reproduced experimental results. The ensemble model demonstrated the ability to predict stick-slip oscillations, and its precision improvement suggests potential applications in structural health monitoring and modal analysis. Overall, the hybrid approach offers advantages over traditional techniques, particularly for systems with stick-slip phenomena, and further investigations will explore limit cycle behavior. The results contribute significantly to the field and have implications for analysis and simulation.

– This thesis utilized physics-informed deep learning to estimate the mechanical and friction parameters of a low-dimensional model. The dynamical model represents a laboratory test rig that replicates the torsional dynamics of drilling operations, incorporating friction effects. Specifically, this study employed the regularized Coulomb model for system identification due to its simplicity and effectiveness. The results demonstrated not only accurate reconstruction of angular velocity time series but also successful estimation of stiffness, damping, and friction parameters. These estimated values were compared with experimental identifications, validating the effectiveness of the methodology.

– This thesis also involves experimental investigations using the apparatus available at the University of Aberdeen. The study focuses on the coupling between torsional and axial oscillations. The experimental setup was modified and adapted to enable the investigation and understanding of this coupling phenomenon. Sensors were utilized to analyze the system's behavior, particularly examining the influence of imposed angular velocity parameters. These experimental investigations provided valuable insights for the study.

Overall, these contributions contribute to the advancement of knowledge in the field of torsional and axial oscillations in drilling systems.

7.2 Recomendations

As a suggestion for future research, the following areas can be explored to build upon the work presented in this doctoral thesis:

– Further exploration and analysis of the coupled dynamics of torsional and axial oscillations in drill-string systems is recommended. This can involve investigating different combinations of system parameters to understand their effects on the coupling behavior. Additionally, it would be beneficial to explore the coupling between torsional and axial vibrations with the lateral mode of vibration, considering the three-dimensional behavior of the drill-string system.

– To enhance the understanding and modeling of drill-string systems, the author suggests integrating additional sensing and monitoring techniques. By incorporating these techniques, a more comprehensive dataset can be obtained, providing detailed information on the behavior and dynamics of the drill-string system.

– To further validate and enhance the proposed identification methodologies in this thesis, it is recommended to conduct experiments where the resistive torque is intentionally kept low. This approach allows for a two-step identification process: first, the estimation of mechanical parameters, and second, the estimation of resistive torque (friction) parameters. By separating these identification steps, the accuracy and reliability of the parameter estimates can be improved, as the influence of resistive torque on the measurements is minimized.

– Development of advanced control strategies to effectively mitigate torsional and axial vibrations in the analyzed systems. These control strategies can be designed based on the identified models obtained in this work. Implementing these advanced control techniques to achieve better vibration suppression and enhanced performance in drill-string systems.

– Application of the proposed identification methods to real-world drilling operations. This would entail evaluating the effectiveness and practicality of the identified models in industrial settings. By implementing these methods in actual drilling operations, one can assess their performance, accuracy, and applicability in practical scenarios.

By directing attention to these specific areas, the author is confident that significant progress can be achieved in the realms of understanding, modeling, and controlling torsional and axial vibrations in drill-string systems, contributing to the drilling operations improvement.

Bibliography

[1] INTERNATIONAL ENERGY AGENCY (IEA). **Oil 2023: The 2023 edition of the IEA's annual medium-term oil market report**. International Energy Agency (IEA), June 2023.

[2] U.S. ENERGY INFORMATION ADMINISTRATION. **Short-term energy outlook**. STEO, July 2023.

[3] KRIESELS, P. C.; KEULTJES, W. J. G.; DUMONT, P.; ISSAN HUNEIDI; OWOEYE, O. O. ; HARTMANN, R. A.. **Cost savings through an integrated approach to drillstring vibration control**. In: SPE/IADC MIDDLE EAST DRILLING TECHNOLOGY CONFERENCE, Abu Dhabi, United Arab Emirates, 1999.

[4] THE EDITORS OF ENCYCLOPAEDIA BRITANNICA. **Petroleum summary**. https://www.britannica.com/summary/petroleum, Accessed on 2023-05-28.

[5] BOURGOYNE JR., A. T.. **Applied Drilling Engineering**. Society of Petroleum Engineers, Dallas, US, 1991.

[6] LIAO, C.; BALACHANDRAN, B. ; KARKOUB, M.. **Drill-string dynamics: Reduced-order models**. In: ASME 2009 INTERNATIONAL MECHANICAL ENGINEERING CONGRESS AND EXPOSITION, Florida, USA, 2009.

[7] MARTINS, L. A.. **Análise dinâmica não linear de colunas de perfuração**. Tese de doutorado, Programa de Pós-graduação em Engenharia Mecânica, Universidade Federal de Uberlândia, Uberlândia, Brasil, 2023.

[8] PIRES, I.; CAYRES, B. C.; PAMPLONA, D. C. ; WEBER, H. I. **Torsional friction-induced vibrations in slender rotating structures**. Mechanisms and Machine Science, 73:3449–3458, 2019.

[9] SRIVASTAVA, S.; TEODORIU, C.. **An extensive review of laboratory scaled experimental setups for studying drill string vibrations and the way forward**. Journal of Petroleum Science and Engineering, 182, 2019.

[10] PATIL, P. A. AND TEODORIU, C. **A comparative review of modelling and controlling torsional vibrations and experimentation using laboratory setups**. Journal of Petroleum Science and Engineering, 112:227–238, 2013.

[11] WIERCIGROCH, M.; KAPITANIAK, M.; VAZIRI, V. ; NANDAKUMAR, K.. **Complex dynamics of drill-strings: Theory and experiments**. In: MATEC WEB OF CONFERENCES, 2018.

[13] LEINE, R.; NIJMEIJER, H. **Dynamics and Bifurcations of Non-smooth Mechanical Systems**. Springer Wiley, Netherlands, 2004.

[14] LIU, X.; VLAJIC, N.; LONG, X.; MENG, G. ; BALACHANDRAN, B.. **Coupled axial-torsional dynamics in rotary drilling with state-dependent delay: Stability and control**. Nonlinear Dynamics, 78:1891–1906, 2014.

[15] CAYEUX, E.; AMBRUS, A.; ØY, L.; HELLELAND, A.; BRUNDTLAND, S. T.; NEVØY, H. ; MORYS, M.. **Analysis of torsional stick-slip situations from recorded downhole rotational speed measurements**. Society of Petroleum Engineers, 2021.

[16] LEINE, R. I.; VAN CAMPEN, D. H. ; DE KRAKER, A.. **Stick-slip vibrations induced by alternate friction models**. Nonlinear Dynamics, 16:41–54, 1998.

[17] SHEN, Y.; ZHANG, Z.; ZHAO, J.; CHEN, W.; HAMZAH, M.; HARMER, R. ; DOWNTON, G.. **The origin and mechanism of severe stick-slip**. Society of Petroleum Engineers, 2017.

[18] GHASEMLOONIA, A.; RIDEOUT, D. G. ; BUTT, S. D.. **A review of drillstring vibration modeling and suppression methods**. Journal of Petroleum Science and Engineering, 131:150–164, 2015.

[19] SALDIVAR, B.; MONDIÉ, S.; NICULESCU, S. I.; MOUNIER, H. ; BOUSSAADA, I.. **A control oriented guided tour in oilwell drilling vibration modeling**. Annual Reviews in Control, 42:100–113, 2016.

[20] GOICOECHEA, H. E.; BUEZAS, F. S. ; ROSALES, M. B.. **A non-linear cosserat rod model for drill-string dynamics in arbitrary borehole geometries with contact and friction**. International Journal of Mechanical Sciences, 157-158, 2019.

[21] LIU, X.; LONG, X.; ZHENG, X.; MENG, G. ; BALACHANDRAN, B.. **Spatial-temporal dynamics of a drill string with complex time-delay effects: Bit bounce and stick-slip oscillations**. International Journal of Mechanical Sciences, 170, 2020.

[22] JANSEN, J. D.; VAN DEN STEEN, L.. **Active damping of self-excited torsional vibrations in oil well drillstrings**. Journal of Sound and Vibration, 179:647–668, 1995.

[23] XIE, D.; HUANG, Z.; MA, Y.; VAZIRI, V.; KAPITANIAK, M. ; WIERCIGROCH, M.. **Nonlinear dynamics of lump mass model of drill-string in horizontal well**. International Journal of Mechanical Sciences, 174, 2020.

[24] LIU, Y.; CHÁVEZ, J. P.; DE SA, R. ; WALKE, S.. **Numerical and experimental studies of stick-slip oscillations in drill-strings**. Nonlinear Dynamics, 90:2959–2978, 2017.

[25] REAL, F. F.; LOBO, D. M.; RITTO, T. G. ; PINTO, F. C.. **Experimental analysis of stick-slip in drilling dynamics in a laboratory test-rig**. Journal of Petroleum Science and Engineering, 2018.

[26] SILVEIRA, M.; WIERCIGROCH, M.. **Low dimensional models for stick-slip vibration of drill-strings**. Journal of Physics: Conference Series, 181:0–8, 2009.

[27] HASNIJEH, S. G.; KARIMPOUR, H. ; POURSINA, M.. **On the random aspect of intermittent stick/slip motion**. Mechanical Systems and Signal Processing, 164, 2022.

[28] RIANE, R.; KIDOUCHE, M.; ILLOUL, R. ; DOGHMANE, M. Z.. **Unknown resistive torque estimation of a rotary drilling system based on kalman filter**. IETE Journal of Research, 2020.

[29] RIANE, R.; KIDOUCHE, M.; DOGHMANE, M. Z. ; ILLOUL, R.. **Modeling of torsional vibrations dynamic in drill-string by using pi-observer**. Proceedings of the 4th International Conference on Electrical Engineering and Control Applications, p. 171–185, 2019.

[30] DE MORAES, L. P. P.; SAVI, M. A.. **Drill-string vibration analysis considering an axial-torsional-lateral nonsmooth model**. Journal of Sound and Vibration, 438:220–237, 2019.

[31] AGUIRRE, L. A.. **Introdução à Identificação de Sistemas**. editora UFMG, Belo Horizonte, 4th edition, 2015.

[32] WORDEN, K.; WONG, C. X.; PARLITZ, U.; HORNSTEIN, A.; ENGSTER, D.; TJAHJOWIDODO, T.; AL-BENDER, F.; RIZOS, D. D. ; FASSOIS, S. D.. **Identification of pre-sliding and sliding friction dynamics: Grey box and black-box models**. Mechanical Systems and Signal Processing, 21:514–534, 2007.

[33] JANOT, A.; YOUNG, P. C. ; GAUTIER, M.. **Identification and control of electro-mechanical systems using state-dependent parameter estimation**. International Journal of Control, 90:643–660, 2017.

[34] BRUNOT, A.; JANOT, M. ; GAUTIER, M.. **Data set and reference models of emps**. 2019.

[35] CHAVES, W. P. F.; AYALA, H. V. H.. **Ensemble grey and black-box nonlinear system identification of a positioning system**. 2020.

[36] LEE, C. Y.; HWANG, S. H.; NAM, E. ; MIN, B. K.. **Identification of mass and sliding friction parameters of machine tool feed drive using recursive least squares method**. International Journal of Advanced Manufacturing Technology, 109:2831–2844, 2020.

[37] AURIOL, J.; SHOR, R.; NICULESCU, S. ; KAZEMI, N.. **Estimating drill string friction parameters: Comparing performance of model-based estimators to a data-driven neural network**. working paper or preprint, 2021.

[38] WORDEN, K.; BARTHORPE, R. J.; CROSS, E. J.; DERVILIS, N.; HOLMES, G. R.; MANSON, G. ; ROGERS, T. J.. **On evolutionary system identification with applications to nonlinear benchmarks**. Mechanical Systems and Signal Processing, 112:194–232, 2018.

[39] MARQUES, F.; FLORES, P.; CLARO, J. C. ; LANKARANI, H. M.. **A survey and comparison of several friction force models for dynamic analysis of multibody mechanical systems**. Nonlinear Dynamics, 86:1407–1443, 2016.

[40] WOJEWODA, J.; STEFANSKI, A.; WIERCIGROCH, M. ; KAPITANIAK, T.. **Hysteretic effects of dry friction: Modelling and experimental studies**. Philosophical Transactions of the Royal Society of London A: Mathematical, Physical and Engineering Sciences, 366:747–765, 2008.

[41] COULOMB, C. A.. **Théorie des machines simples, en ayant égard au frottement de leurs parties, et à la roideur des cordages. Mémoire de Mathématique et de Physique**. Paris, 1785.

[42] STRIBECK, R.. **Die wesentlichen eigenschaften der gleitund rollenlager—the key qualities of sliding and roller bearings**. Zeitschrift des Vereines Deutscher Ingenieure, 46:1342–1348, 1903.

[43] TUSTIN, A.. **The effects of backlash and of speed-dependent friction on the stability of closed-cycle control systems**. J. Inst. Electr. Eng., 94:143–151, 1947.

[44] DAHL, P.. **A solid friction model**. Technical Report TOR-0158 (3107-18)-1, The Aerospace Corporation, El Segundo, CA., 1968.

[45] STEFAŃSKI, A.; WOJEWODA, J.; WIERCIGROCH, M. ; KAPITANIAK, T.. **Chaos caused by non-reversible dry friction**. Chaos, Solitons and Fractals, 16:661–664, 2003.

[46] STEFAŃSKI, A.; WOJEWODA, J.; WIERCIGROCH, M. ; KAPITANIAK, T.. **Regular and chaotic oscillations of friction force**, 2006.

[47] ISERMANN, R.; MÜNCHHOF, M.. **Identification of Dynamic Systems: An Introduction with Applications**. Springer, Verlag, 1st edition, 2011.

[49] VAN DEN HOF, P.. **Closed-loop issues in system identification**. Annual Reviews in Control, 22:173–186, 1998.

[50] ENGEL. **Funktions und abgleichbeschreibung für 4-quadrantenservoverstärker in getakteter c-mos-transistortechnik**, 1998.

[51] ANDERSSON, J. A. E.; GILLIS, J.; HORN, G.; RAWLINGS, J. B. ; DIEHL, M.. **Casadi: a software framework for nonlinear optimization and optimal control**. Math. Prog. Comp., 11:1–36, 2019.

[52] WÄCHTER, A.; BIEGLER, L. T.. **On the implementation of an interior-point filter line-search algorithm for large-scale nonlinear programming**. Math Program, 106:25–57, 2006.

[53] PACKARD, N. H.; CRUTCHFIELD, J. P.; FARMER, J. D. ; SHAW, R. S.. **Geometry from a time series**. Physical Review Letters, 45:712–716, 1980.

[54] AGUIRRE, L. A.; BILLINGS, S. A.. **Validating identified nonlinear models with chaotic dynamics**. International Journal of Bifurcation and Chaos, 4(1):109–125, 1994.

[55] AGUIRRE, L. A.; BILLINGS, S. A.. **Retrieving dynamical invariants from chaotic data using narmax models**. International Journal of Bifurcation and Chaos, 2:449–474, 1995.

[56] WITKOWSKI, K.; KUDRA, G.; SKURATIVSKYI, S.; WASILEWSKI, G. ; AWREJCEWICZ, J.. **Modeling and dynamics analysis of a forced two-degree-of-freedom mechanical oscillator with magnetic springs**. Mechanical Systems and Signal Processing, 148:107138, 2021.

[57] RITTO, T. G.; AGUIAR, R. R. ; HBAIEB, S.. **Validation of a drill string dynamical model and torsional stability**. Meccanica, 52:959–2967, 2017.

[58] AVCI, O.; ABDELJABER, O.; KIRANYAZ, S.; HUSSEIN, M.; GABBOUJ, M. ; INMAN, D. J.. **A review of vibration-based damage detection in civil structures: From traditional methods to machine learning and deep learning applications**. Mechanical Systems and Signal Processing, 147:129107077, 2021.

[59] CANDON, M.; LEVINSKI, O.; OGAWA, H.; CARRESE, R. ; MARZOCCA, P.. **A nonlinear signal processing framework for rapid identification and diagnosis of structural freeplay**. Mechanical Systems and Signal Processing, 163:107999, 2022.

[60] LIU, D.; LUO, M.; ZHANG, Z.; HU, Y. ; ZHANG, D.. **Operational modal analysis based dynamic parameters identification in milling of thin-walled workpiece**. Mechanical Systems and Signal Processing, 167:108469, 2022.

[61] RAISSI, M.; WANG, Z.; TRIANTAFYLLOU, M. S. ; KARNIADAKIS, G.. **Deep learning of vortex induced vibrations**. Journal of Fluid Mechanics, 25:119–137, 2018.

[62] WIERCIGROCH, M.; KAPITANIAK, M.; VAZIRI, V. ; NANDAKUMAR, K.. **Complex dynamics of drill-strings: Theory and experiments**. MATEC Web of Conferences, 211:01002, 2018. Published online on 10 October 2018.

[63] KAPITANIAK, M.; VAZIRI, V.; PÁEZ CHÁVEZ, J. ; WIERCIGROCH, M.. **Experimental studies of forward and backward whirls of drill-string**. Mechanical Systems and Signal Processing, 100:454–465, 2018.

[64] KAPITANIAK, M.; VAZIRI, V.; PÁEZ CHÁVEZ, J.; NANDAKUMAR, K. ; WIERCIGROCH, M.. **Unveiling complexity of drill–string vibrations: Experiments and modelling**. International Journal of Mechanical Sciences, 101–102:324–337, 2015.

[65] PIRES, I.; WEBER, H. I. ; AYALA, H. V. H.. **Nonlinear ensemble gray and black-box system identification of friction-induced vibrations in slender rotating structures**. Mechanical Systems and Signal Processing, 186, 2023.

[66] KHULIEF, Y. A.; AL-SULAIMAN, F. A.. **Laboratory investigation of drillstring vibrations**. Proceedings of the Institution of Mechanical Engineers, Part C: Journal of Mechanical Engineering Science, 223(10):2249–2262, 2009.

[67] KOVALYSHEN, Y.. **Experiments on stick-slip vibrations in drilling with drag bits**. In: PAPER PRESENTED AT THE 48TH U.S. ROCK MECHANICS/GEOMECHANICS SYMPOSIUM, Minneapolis, Minnesota, June 2014.

[68] LOEKEN, E. A.; TRULSEN, A.; HOLSAETER, A. M.; WIKTORSKI, E.; SUI, D. ; EWALD, R.. **Design principles behind the construction of an autonomous laboratory-scale drilling rig**. IFAC-PapersOnLine, 51(8):62–69, 2018.

[69] LIN, T.; ZHANG, Q.; LIAN, Z.; XIAO, Z.; WANG, T.; LI, G. ; DING, J.. **Experimental study on vibrational behaviors of horizontal drillstring**. Journal of Petroleum Science and Engineering, 164:311–319, 2018.

[70] INMAN, D. J.. **Engineering Vibration**. Prentice-Hall, Upper Saddle River, NJ, 4th ed edition, 2014.

[71] PIRES, I. **Torsional friction-induced vibrations in slender rotating structures**. Dissertação de mestrado, Departamento de Engenharia Mecânica, Pontifícia Universidade Católica do Rio de Janeiro, Rio de Janeiro, 2019.